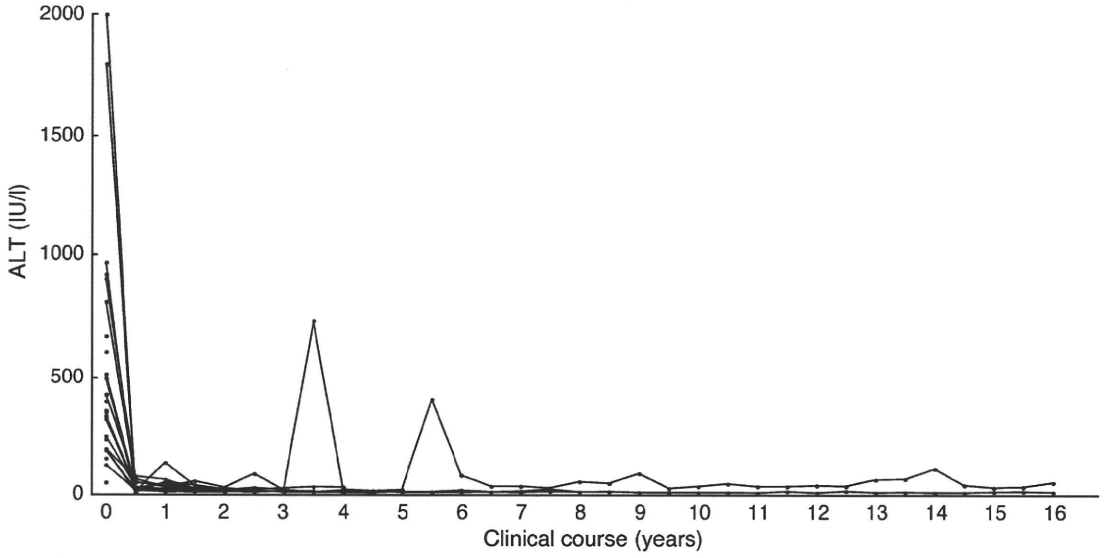

Fig. 3 Long-term changes in ALT levels after the start of treatment in all patients

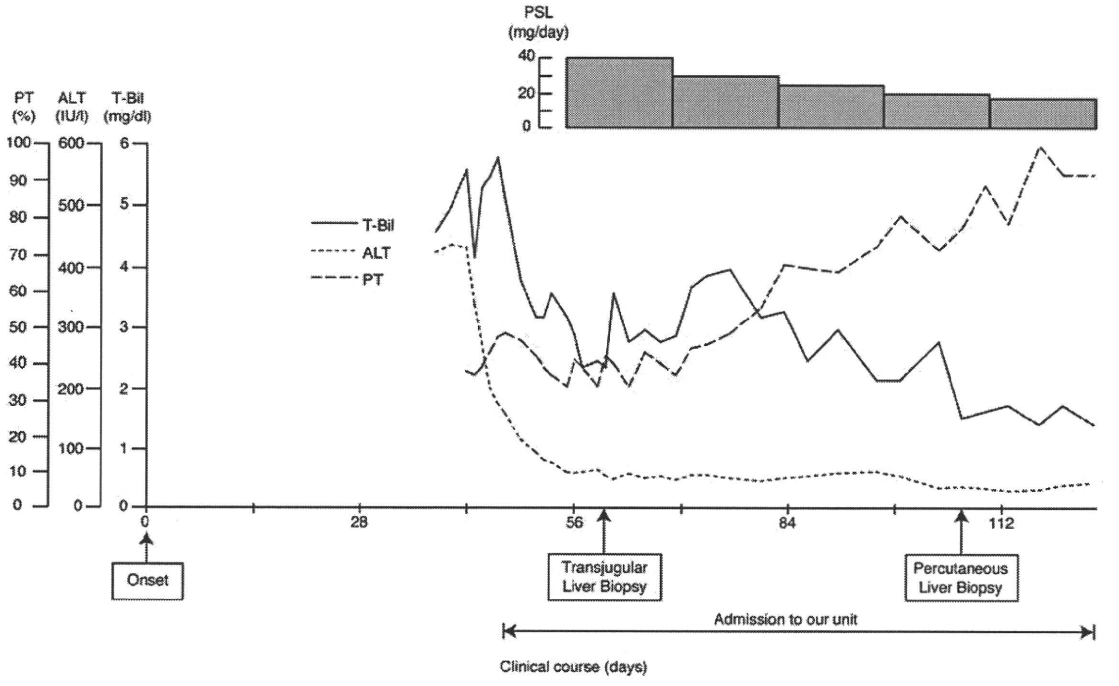

Fig. 4 Clinical course of a 26-year-old female patient (patient 20, responder). She suffered from cryptogenic acute hepatitis showing 35% of PT activity after a month of treatment and was admitted to our unit. Corticosteroid was administered, and her liver function tests gradually improved

and treat acute onset AIH patients before they develop severe and fulminant disease. AIH patients with low PT activity have very severe and advanced histology and present impaired hepatocellular regeneration, which is associated with resistance to immunosuppressive therapy.

In conclusion, we should be aware of the possibility that acute onset AIH patients exist among those with cryptogenic hepatitis, and that this condition can cause severe hepatitis and fulminant hepatic failure with a poor prognosis if the diagnosis was delayed and sufficient immunosuppressive therapy could not be introduced at an early stage. However, making the diagnosis of acute onset AIH is very difficult because there is no gold standard for it. It is most important to exclude other causes systematically, remember acute onset AIH in the differential diagnosis and then apply the scoring system, and comprehensive evaluations of clinical,

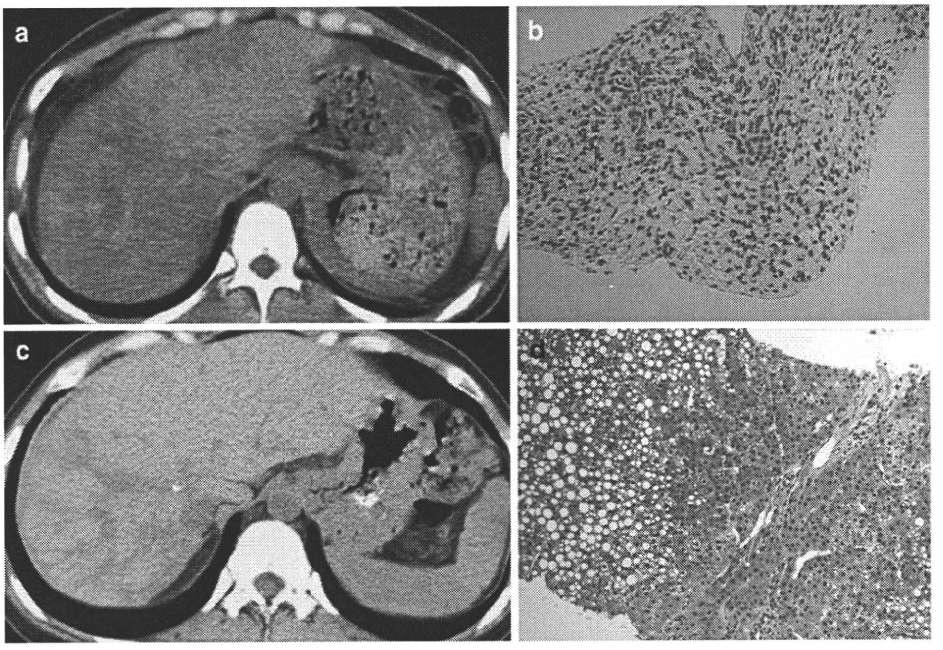

Fig. 5 CT and histological findings of a responder (patient 20). At admission to our unit, CT scan showed marked liver atrophy with heterogeneous hypoattenuation areas (**a**), suggesting massive hepatic necrosis, and liver histology showed massive necrosis without plasma cell accumulation, compatible with acute autoimmune hepatitis (**b**). Two months after the administration of corticosteroid, CT scan showed enlargement of the left lobe and a decrease in the hypoattenuation areas (**c**), and liver histology showed simple steatosis with minimal necroinflammatory change (**d**)

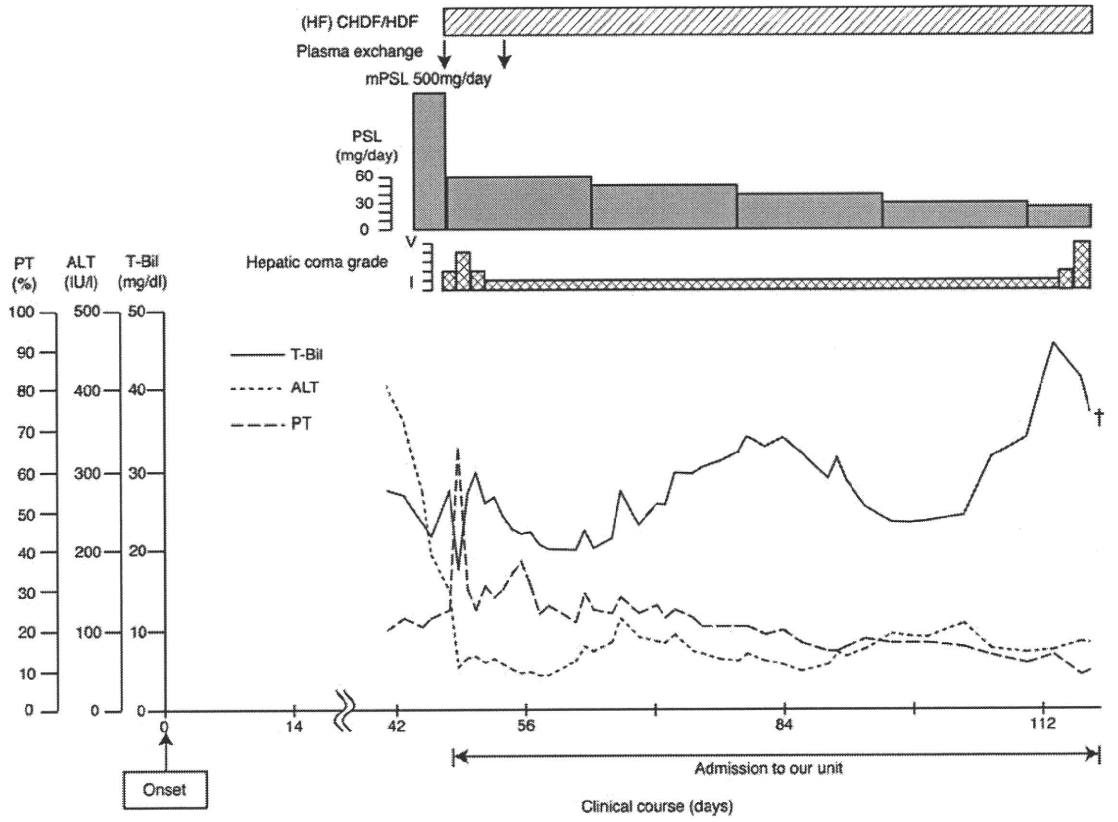

Fig. 6 Clinical course of a 70-year-old female patient (patient 23, non-responder). She suffered from cryptogenic acute hepatitis showing 20% of PT activity and 28 mg/dl of T-Bil after 50 days of treatment and was admitted to our unit. Corticosteroid was administered in combination with artificial liver support: high flow (HF)-continuous hemodiafiltration (CHDF) and plasma exchange. Her hepatic encephalopathy improved to grade I, but liver function tests did not improve. She died 3 months after admission because of hepatic failure

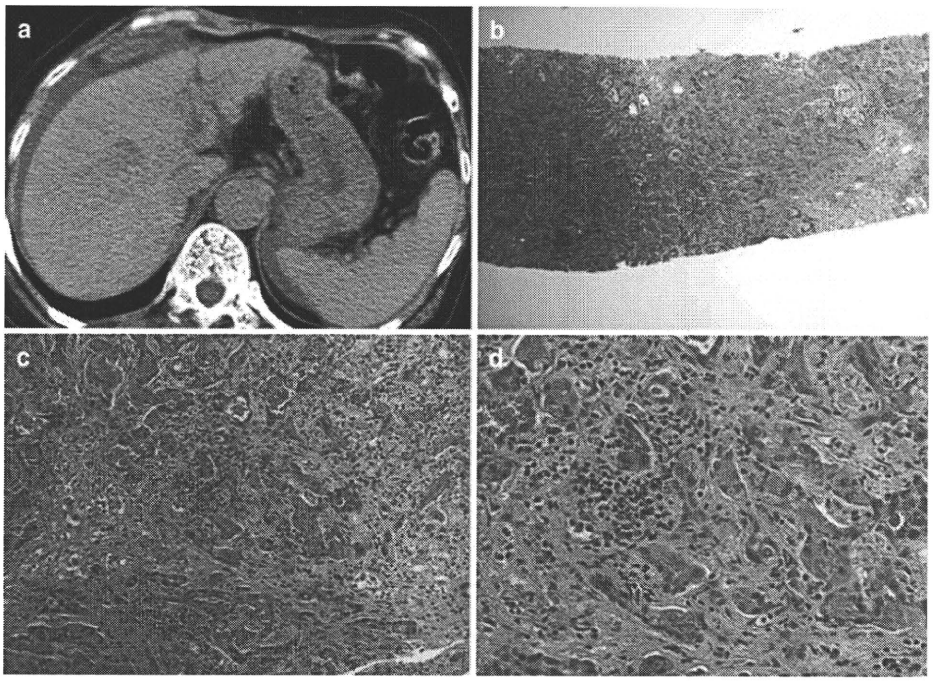

Fig. 7 CT and histological findings of non-responder (patient 23). At admission she presented grade III hepatic encephalopathy, and CT scan showed mild liver atrophy (**a**). Post mortem liver histology showed massive necrosis with plasma cell accumulation, compatible with acute autoimmune hepatitis (**b–d**)

biochemical, radiological and histological features are necessary for early diagnosis. Especially precise pathological evaluation plays an important role in the differential diagnosis: recognition of severe centrizonal necrosis with or without plasma cell accumulation. We should study and recognize the pathological characteristics of acute onset AIH. The prognosis might indeed be improved without liver transplantation by the introduction of sufficient immunosuppressive therapy at an early stage. Multicenter studies are also needed to clarify the features of severe and fulminant AIH and define the treatment strategies.

Acknowledgments We are indebted to all our colleagues at the liver unit of our hospital who cared for the patients described herein.

Conflict of interest No conflicts of interest exist.

References

1. Czaja AJ. Autoimmune hepatitis: evolving concepts and treatment strategies. Dig Dis Sci. 1995;40:435–56.
2. Czaja AJ, Carpenter HA. Sensitivity, specificity and predictability of biopsy interpretations in chronic hepatitis. Gastroenterology. 1993;105:1824–32.
3. Czaja AJ, Davis GL, Ludwig J, Baggenstoss AH, Taswell HF. Autoimmune features as determinants of prognosis in steroid-treated chronic active hepatitis of uncertain etiology. Gastroenterology. 1983;85:713–7.
4. Crapper RM, Bhathal PS, Mackay IR, Frazer IH. "Acute" autoimmune hepatitis. Digestion. 1986;34:216–25.
5. Amontree JS, Stuart TD, Bredfeldt JE. Autoimmune chronic active hepatitis masquerading as acute hepatitis. J Clin Gastroenterol. 1989;11:303–7.
6. Nikias GA, Batts KP, Czaja AJ. The nature and prognostic implications of autoimmune hepatitis with an acute presentation. J Hepatol. 1994;21:866–71.
7. Porta G, Da Costa Gayotto LC, Alvarez F. Anti-liver-kidney microsome antibody-positive autoimmune hepatitis presenting as fulminant liver failure. J Ped Gastroenterol Nutr. 1990; 11:138–40.
8. Alvarez F, Berg PA, Bianchi FB, Bianchi L, Burroughs AK, Cancado EL, et al. International Autoimmune Hepatitis Group report: review of criteria for diagnosis of autoimmune hepatitis. J Hepatol. 1999;31:929–38.
9. Fujiwara K, Mochida S, Matsui A, Nakayama N, Nagoshi S, Toda G. Intractable Liver Diseases Study Group of Japan Fulminant hepatitis and late onset hepatic failure in Japan. Hepatol Res. 2008;38:646–57.
10. Ichai P, Samuel D. Etiology and prognosis of fulminant hepatitis in adults. Liver Transpl. 2008;14:S67–79.
11. Lee WM, Squires RH Jr, Nyberg SL, Doo E, Hoofnagle JH. Acute liver failure: summary of a workshop. Hepatology. 2008;47:1401–15.
12. Lefkowitch JH, Apfelbaum TF, Weinberg L, Forester G. Acute liver biopsy lesions in early autoimmune ('lupoid') chronic active hepatitis. Liver. 1984;4:379–86.
13. Ohta Y, Onji M. Clinical characteristics of autoimmune hepatitis in Japan. In: Nishioka M, Toda G, Zeniya M, editors. Autoimmune hepatitis. Amsterdam: Elsevier; 1993. p. 45–53.
14. Fujiwara K, Fukuda Y, Yokosuka O. Precise histological evaluation of liver biopsy specimen is indispensable for diagnosis and treatment of acute onset autoimmune hepatitis. J Gastroenterol. 2008;43:951–8.
15. Desmet VJ, Gerber M, Hoofnagle JH, Manns M, Scheuer PJ. Classification of chronic hepatitis: diagnosis, grading and staging. Hepatology. 1994;19:1513–20.

16. Maria VAJ, Victorino RMM. Development and validation of a clinical scale for the diagnosis of drug-induced hepatitis. Hepatology. 1997;26:664–9.
17. Kaymakoglu S, Cakaloglu Y, Demir K, Turkoglu S, Badur S, Gurel S, et al. Is severe cryptogenic chronic hepatitis similar to autoimmune hepatitis? J Hepatol. 1998;28:78–83.
18. Potthoff A, Deterding K, Trautwein C, Flemming P, Strassburg CP, Manns MP, et al. Steroid treatment for severe acute cryptogenic hepatitis. Z Gastroenterol. 2007;45:15–9.
19. Bernal W, Ma Y, Smith HM, Portmann B, Wendon J, Vergani D. The significance of autoantibodies and immunoglobulins in acute liver failure: a cohort study. J Hepatol. 2007;47:664–70.
20. Ferrari R, Pappas G, Agostinelli D, Muratori P, Muratori L, Lenzi M, et al. Type 1 autoimmune hepatitis: patterns of clinical presentation and differential diagnosis of the 'acute' type. QJM. 2004;97:407–12.
21. Burgart LJ, Batts KP, Ludwig J, Nikias GA, Czaja AJ. Recent onset autoimmune hepatitis. Biopsy findings and clinical correlations. Am J Surg Pathol. 1995;19:699–708.
22. Abe M, Onji M, Kawai-Ninomiya K, Michitaka K, Matsuura B, Hiasa Y, et al. Clinicopathologic features of the severe form of acute type 1 autoimmune hepatitis. Clin Gastroenterol Hepatol. 2007;5:255–8.
23. Tokumoto Y, Onji M. Acute-onset autoimmune hepatitis. Intern Med. 2007;46:1–2.
24. Singh R, Nair S, Farr G, Mason A, Perrillo R. Acute autoimmune hepatitis presenting with centrizonal liver disease: case report and review of the literature. Am J Gastroenterol. 2002;97:2670–3.
25. Hofer H, Oesterreicher C, Wrba F, Ferenci P, Penner E. Centrilobular necrosis in autoimmune hepatitis: a histological feature associated with acute clinical presentation. J Clin Pathol. 2006;59:246–9.
26. Kessler WR, Cummings OW, Eckert G, Chalasani N, Lumeng L, Kwo PY. Fulminant hepatic failure as the initial presentation of acute autoimmune hepatitis. Clin Gastroenterol Hepatol. 2004;2:625–31.
27. Misdraji J, Thiim M, Graeme-Cook FM. Autoimmune hepatitis with centrilobular necrosis. Am J Surg Pathol. 2004;28:471–8.
28. Okuda K, Mitchell DG, Itai Y, Ariyama J. Hepatobiliary diseases. London: Blackwell Science; 2001. p. 97–100.
29. Murakami T, Baron RL, Peterson MS. Liver necrosis and regeneration after fulminant hepatitis: pathologic correlation with CT and MR findings. Radiology. 1996;198:239–42.
30. Muto Y. Imaging diagnosis of fulminant hepatitis. Liver failure. Tokyo: Nihon Iji Shimposha; 1994. p. 164.
31. O'Grady JG, Alexander GJ, Hayllar KM, Williams R. Early indicators of prognosis in fulminant hepatic failure. Gastroenterology. 1989;97:439–45.
32. Miyake Y, Iwasaki Y, Terada R, Onishi T, Okamoto R, Sakai N, et al. Clinical characteristics of fulminant-type autoimmune hepatitis: an analysis of eleven cases. Aliment Pharmacol Ther. 2006;23:1347–53.
33. Czaja AJ, Rakela J, Ludwig J. Features reflective of early prognosis in corticosteroid-treated severe autoimmune chronic active hepatitis. Gastroenterology. 1988;95:448–53.
34. Czaja AJ. Corticosteroids or not in severe acute or fulminant autoimmune hepatitis: therapeutic brinksmanship and the point beyond salvation. Liver Transpl. 2007;13:953–5.

VIROLOGY JOURNAL

SHORT REPORT Open Access

Inhibitory effects on HAV IRES-mediated translation and replication by a combination of amantadine and interferon-alpha

Lingli Yang[1,4†], Tomoko Kiyohara[2†], Tatsuo Kanda[1*†], Fumio Imazeki[1], Keiichi Fujiwara[1], Verena Gauss-Müller[3], Koji Ishii[2], Takaji Wakita[2], Osamu Yokosuka[1]

Abstract

Hepatitis A virus (HAV) causes acute hepatitis and sometimes leads to fulminant hepatitis. Amantadine is a tricyclic symmetric amine that inhibits the replication of many DNA and RNA viruses. Amantadine was reported to suppress HAV replication, and the efficacy of amantadine was exhibited in its inhibition of the internal ribosomal entry site (IRES) activities of HAV. Interferon (IFN) also has an antiviral effect through the induction of IFN stimulated genes (ISG) and the degradation of viral RNA. To explore the mechanism of the suppression of HAV replication, we examined the effects of the combination of amantadine and IFN-alpha on HAV IRES-mediated translation, HAV replicon replication in human hepatoma cell lines, and HAV KRM003 genotype IIIB strain replication in African green monkey kidney cell GL37. IFN-alpha seems to have no additive effect on HAV IRES-mediated translation inhibition by amantadine. However, suppressions of HAV replicon and HAV replication were stronger with the combination than with amantadine alone. In conclusion, amantadine, in combination of IFN-alpha, might have a beneficial effect in some patients with acute hepatitis A.

Short report

Hepatitis A virus (HAV), a member of the family Picornaviridae, causes acute hepatitis and occasionally fulminant hepatitis, a life-threatening disease. As the broad epidemiological picture of hepatitis A changes, the public health importance of this disease is being increasingly recognized [1]. It is a significant cause of morbidity worldwide, although the mortality rate due to hepatitis A is low (improved intensive care and transplantation have contributed to a reduction in deaths). Improved sanitation and living standards mean that fewer countries remain highly endemic, but the risk of HAV infection is present in countries lacking HAV immunity or where the endemicity of hepatitis A is low or intermediate [1]. In such situations, these outbreaks can prove to be long and difficult to control. Vaccination and informing the general public about good hygienic measures are important for the prevention of HAV infection, but new therapeutic options are also desirable.

Amantadine, a tricyclic symmetric amine, inhibits HAV replication *in vitro* [2]. We previously reported that amantadine inhibits hepatitis A virus internal ribosomal entry site (IRES)-mediated translation in human hepatoma cells [2]. Interferons (IFNs) also exhibit antiviral effects against HAV infection [2,3]. In the present study, we examined the effects of amantadine with or without IFN-alpha, on HAV IRES activities, HAV subgenomic replicon replication and HAV replication *in vitro* as a proof of concept for the development of a more effective treatment to control HAV infection.

First, we evaluated the cytotoxicity of amantadine and IFN-alpha by 3-(4,5-dimethylthiazol-2-yl)-5-(3-carboxymethoxyphenyl)-2-(4-sulfophenyl)-2H-tetrazolium, inner salt (MTS) assay. Amantadine concentrations in a range of 1 - 125 μg/mL and those of 1 - 150 μg/mL for 12-h incubation were non-toxic for Huh7 cells and for HuhT7 cells, respectively (Figures 1A and 1B). Amantadine could be incubated for a short time, e.g., 12 h, with the cells, and then the dose of amantadine could be

* Correspondence: kandat-cib@umin.ac.jp
† Contributed equally
[1]Department of Medicine and Clinical Oncology, Graduate School of Medicine, Chiba University, 1-8-1 Inohana, Chuo-ku, Chiba 260-8670, Japan
Full list of author information is available at the end of the article

BioMed Central

© 2010 Yang et al; licensee BioMed Central Ltd. This is an Open Access article distributed under the terms of the Creative Commons Attribution License (http://creativecommons.org/licenses/by/2.0), which permits unrestricted use, distribution, and reproduction in any medium, provided the original work is properly cited.

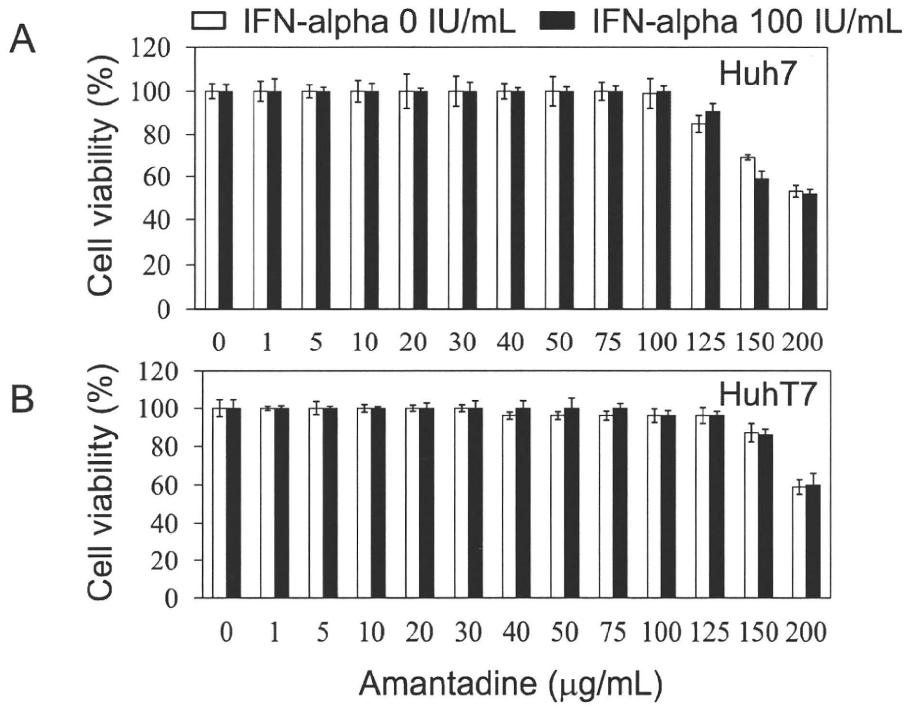

Figure 1 Effects of amantadine on cell growth and viability. MTS assays of cells 12 h after treatment with amantadine with or without 100 U/mL interferon (IFN)-alpha. (A) Huh7 cells. (B) HuhT7 cells. Data are expressed as mean ± SD.

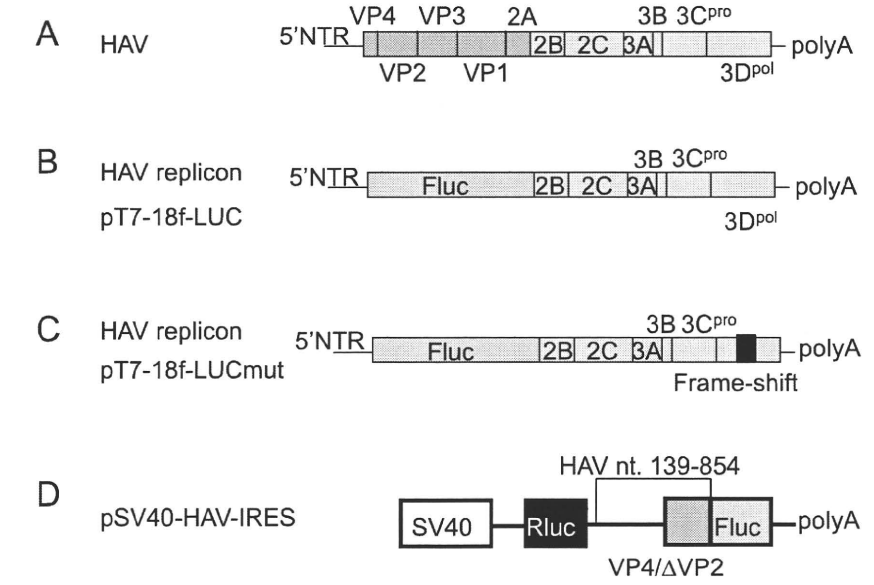

Figure 2 Structures of reporter constructs used in this study. (A) Structure of HAV genome. **(B)** Structure of the replication-competent HAV replicon (HAV replicon) pT7-18f-LUC, which contains an open-reading frame of firefly luciferase (Fluc) flanked by the first four amino acids of HAV polyprotein and by 12 C-terminal amino acids of VP1. This segment is followed by P2 and P3 domains of HAV polyprotein (HAV strain HM175 18f) [9,10]. **(C)** Structure of replication-incompetent HAV replicon (mut) (mut-HAV replicon) pT7-18f-LUCmut, which contains a frame-shift mutation in the polymerase 3 D [9,10]. **(D)** Bicistronic reporter constructs: pSV40-HAV IRES was described previously [2,4]. It encodes the Renilla luciferase genes (Rluc), the internal ribosomal entry site (IRES) HAV HM175, and the firefly luciferase gene (Fluc) under the control of the simian virus 40 promoter (SV40).

increased to higher than 100 μg/mL. With the combination of amantadine and 100 IU/mL IFN-alpha, we did not observe increased cytotoxicity compared with amantadine alone.

We previously reported that the introduction of siRNA targeted against the 5'NTR region of HAV HM175 inhibits HAV IRES-mediated translation and HAV replication [4]. Interestingly, amantadine and IFN also inhibited HAV IRES-mediated translation and HAV replication [2,3,5-8]. Accordingly, we planned to identify more effective strategies for suppressing HAV IRES-mediated translation and HAV replication. IRES is an attractive target for antivirals because HAV IRES is located in the 5'NTR region, the most conserved region among HAV strains. In the present study, we evaluated the HAV antiviral activity of amantadine and IFN-alpha. We initially examined the effects of this combination on HAV IRES-mediated translation using a luciferase reporter assay. Huh7 cells were transfected with pSV40-HAV IRES reporter vector, encoding SV40 promoter driven-*Renilla reniformis* and firefly luciferase, separated by HAV-IRES (Figure 2) [2], and treated with amantadine and/or IFN-alpha. Inhibition of luciferase activity at different levels was observed with amantadine with or without 100 IU/mL IFN-alpha (Figure 3A). Although the strongest suppression was noted with the combination of 10 μg/mL amantadine and 100 IU/mL IFN-alpha, IFN-alpha showed no additive effect on the translation inhibition by 50-100 μg/mL amantadine. This finding prompted us to examine whether IFN-alpha has additive suppression of HAV replicon replication by amantadine. We have reported that RNA replication of HAV can be analyzed in a DNA-based replicon system using HuhT7 cells that stably express T7-RNA polymerase in the cytoplasm (Figure 1) [9-11]. The luciferase activities determined after transfection of replicon DNA are a direct measure of RNA translation and replication. This is because replication in positive-stranded RNA viruses can be easily assessed with a viral replicon carrying the luciferase gene in place of viral structural genes. Moreover, luciferase activity due to translation or translation and replication can be evaluated when the transfection of a replication-competent replicon (HAV replicon) is compared with that of a replication-incompetent replicon (mut) (mut-HAV replicon) [8].

To further determine the effects of the combination of amantadine and IFN-alpha on HAV replication, we transfected the HAV replicon or mut-HAV replicon into HuhT7 cells, and the drugs were added 24 h later. Reporter assays were performed 48 or 72 h after transfection. The transfection efficacy of HAV replicon was estimated as 20-30% in our systems. Luciferase activity was normalized with respect to the protein concentration of cell

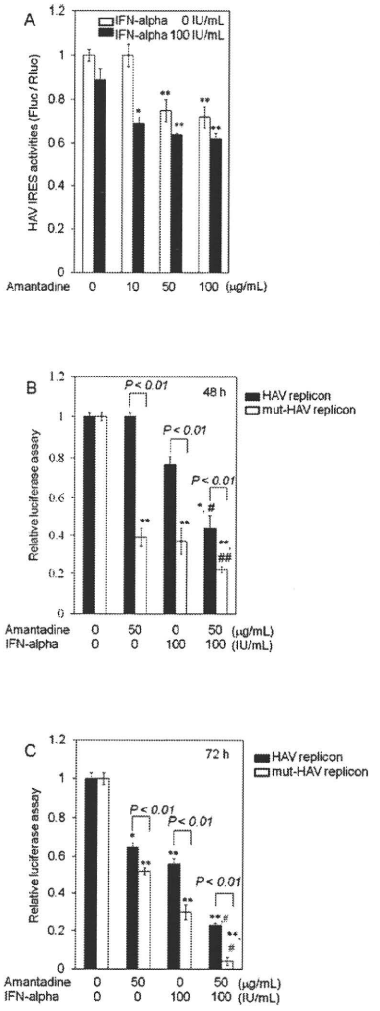

Figure 3 (A) Effects of amantadine with or without interferon on the hepatitis A virus (HAV) internal ribosomal entry site (IRES) activities in Huh7 cells. Approximately 2 × 10^5 cells were seeded on a 6-well tissue culture plate (Iwaki Glass, Tokyo, Japan) 24 h prior to transfection. pSV40-HAV-IRES (0.3 μg) was transfected into Huh7 cells using the Effectene transfection reagent (Qiagen, Tokyo, Japan). 24 h after transfection, amantadine and/or IFN in various concentrations was added to cells. 48 h after transfection, cell extracts were prepared, and luciferase assays were performed using the Dual Luciferase assay system (Toyo Ink, Tokyo, Japan) according to the manufacturer's instructions [2]. For controlling the variations in transcription, IRES activity was assessed by measuring the ratio of *Renilla* and firefly luciferases. All samples were run in triplicate. *Renilla* and firefly luciferase activities were measured as relative light units using a luminescencer (JNRII-AB-2300; ATTO, Tokyo, Japan). **(B, C) Effects of amantadine with or without interferon on the HAV subgenomic replicon replication in HuhT7 cells. (B)** 48 h after transfection and **(C)** 72 h after transfection. Black columns, replication-competent HAV replicon; white columns, replication-incompetent HAV replicon (mut). Relative luciferase activities without any treatments were set at 1. Data are expressed as mean (columns) ± SD (vertical lines). *$P < 0.05$ and **$P < 0.01$, compared with untreated control by Student's t test. #$P < 0.01$ and ## $P < 0.05$, compared with amantadine alone or IFN-alpha alone by Student's t test.

lysates. In this DNA-based system, 48 h after transfection, the replication rates of the HAV replicon were 100%, 77%, and 44% compared to those of control when treated with amantadine alone, IFN alone, and their combination, respectively (Figure 3B). On the other hand, since the mut-HAV replicon cannot replicate, the luciferase activity (39%, 37%, and 22% compared to those of control for the same test conditions, respectively) is due to translation of the viral RNA and not replication. Amantadine alone showed 52% at 72 h, higher than 37% at 48 h, supporting the notion that amantadine might suppress translation of the viral RNA. Suppression effects of these treatments were stronger in the mut-HAV replicon than in the HAV replicon. These findings support our observation of the suppression of HAV IRES-mediated translation by amantadine and IFN-alpha. Suppression effects at 48 h after transfection by the combination of amantadine and IFN-alpha against HAV replication were stronger than those by amantadine or IFN-alpha monotreatment. IFN-alpha was more effective than amantadine against the HAV replicon ($P = 0.0027$) (Figure 3B).

Seventy-two hours after transfection, the replication rates of the HAV replicon were 65%, 56%, and 23% compared to those of control when treated with amantadine alone, IFN-alpha alone, and their combination, respectively (Figure 3C). The replication rates of the mut-HAV replicon were 52%, 30%, and 4% of those of control, respectively. IFN-alpha was more effective than amantadine against the replication of HAV replicon or mut-HAV replicon ($P < 0.001$ or $P < 0.001$). Suppression effects of the combination of amantadine and IFN-alpha at 72 h post-transfection were stronger than those of amantadine or IFN-alpha monotreatment. Suppression effects of these treatments were stronger in the mut-HAV replicon than in the HAV replicon. Moreover, it is important to note that the effects of this combination were observed at earlier time points (Figure 3C).

Next, we performed an infectivity assay using the virus to investigate the effects of combination of amantadine and IFN-alpha on tissue culture-adapted HAV strain KRM003 (genotype IIIB, accession no. L20536) propagation in African green monkey kidney GL37 cells [12-14]. GL37 cell monolayers in 96-well culture plates were infected with HAV at a multiplicity of infection (MOI) of 5 or 50 for 1 h at 37°C in a CO_2 incubator. Without removing the inoculum, drug-containing media were added to appropriate wells. The final concentrations of amantadine, IFN-alpha, and their combination were 50 μg/ml, 100 IU/ml and 50 μg/ml of amantadine and 100 IU/ml of IFN-alpha, respectively. After incubation for 72 h, infected cells were evaluated with ELISA. Suppression of HAV replication by the combination of amantadine and IFN-alpha was stronger than those of amantadine alone, IFN-alpha alone, and untreated control (Figure 4).

IFNs are proteins induced by lymphocytes and other cells including hepatocytes in response to viruses such as HAV. In virus-infected cells, dsRNA activates antiviral interferon pathways and the production of IFN type I. The secreted IFN type I induces a positive feedback loop that results in the expression of interferon-stimulated genes (ISGs), including RNase L and protein kinase R (PKR) [15]. Our study supports the fact that the administration of IFN-alpha suppresses HAV replication through HAV IRES mediated-translation and other mechanisms and that, on the other hand, amantadine suppresses HAV replication mainly through HAV IRES mediated-translation.

There are several reports concerning HAV suppressing intracellular dsRNA-induced retinoic acid-inducible gene I (RIG-I)-mediated IFN regulatory factor 3 (IRF-3) activation to block induction of IFN [16,17]. Yang et al. reported that HAV proteins interact with mitochondrial antiviral signaling protein, an essential component of virus-activated signaling pathways that induce protective IFN responses [18]. However, in this study, the

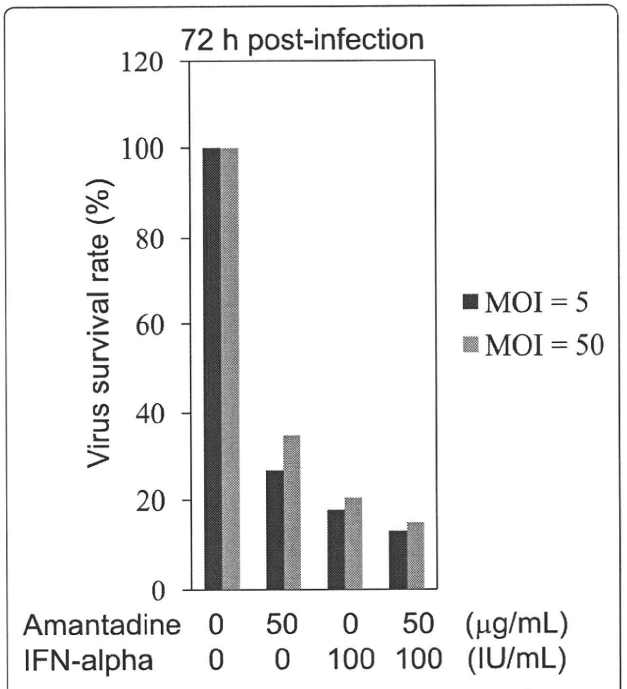

Figure 4 Effects of amantadine with or without interferon on HAV KRM003 genotype IIIB strain replication in African green monkey kidney cell GL37. GL37 cell monolayers in 96-well culture plates were infected with HAV [at a multiplicity of infection (MOI) of 5 or 40] for 1 h at 37°C in a CO_2 incubator. Amantadine and/or IFN was added to cells. After the incubation for 72 h, infected cells were evaluated with ELISA. The rate of virus survival was measured using this equation: Virus survival rate (%) = 100 × Absorbance with drug/Absorbance without drug.

administration of exogenous IFN-alpha could suppress HAV replication, although endogenous IFNs produced by cells also may play an important role in inhibiting viral replication. Further studies will be needed.

Amantadine inhibits the replication of many DNA and RNA viruses and is also used as a drug for the treatment of Parkinson's disease [2]. It is known that the M2 protein of influenza A virus is a target of amantadine [19]. Furthermore, it has been reported to inhibit HAV IRES-mediated translation and replication by our group and other researchers [2,3,5-8].

Therefore, we examined the possibilities of the combination of amantadine and IFN-alpha against HAV because these two drugs were previously reported to be effective against HAV [2,3,5-8]. To our knowledge, this is the first study demonstrating that a combination of amantadine and IFN-alpha can suppress HAV replication more effectively than amantadine or IFN-alpha alone.

Abbreviations

HAV: hepatitis A virus; **IRES**: internal ribosomal entry site; **IFN**: interferon; **MTS**: 3-(4,5-dimethylthiazol-2-yl)-5-(3-carboxymethoxyphenyl)-2-(4-sulfophenyl)-2H-tetrazolium, inner salt.

Acknowledgements

We thank Dr. S. U. Emerson for providing the plasmids. This work was supported by grants for Scientific Research 21590829, 21590828, and 21390225 from the Ministry of Education, Culture, Sports, Science, and Technology, Japan (TK, FI, and OY), a grant from the Ministry of Health, Labor, and Welfare of Japan (OY), and a grant from Chiba University Young Research-Oriented Faculty Member Development Program in Bioscience Areas (TK).

Author details

[1]Department of Medicine and Clinical Oncology, Graduate School of Medicine, Chiba University, 1-8-1 Inohana, Chuo-ku, Chiba 260-8670, Japan. [2]Department of Virology II, National Institute of Infectious Diseases, 4-7-1, Gakuen, Musashi-Murayama, Tokyo 280-0011, Japan. [3]Institute of Medical Molecular Biology, University of Lübeck, Ratzeburger Allee 160, D-23538 Lübeck, Germany. [4]Department of Dermatology, Graduate School of Medicine, Osaka University, Osaka 565-0871, Japan.

Authors' contributions

LY, Tatsuo Kanda, FI and OY conceived and designed the study. LY, Tomoko Kiyohara and Tatsuo Kanda performed the experiments. LY, Tomoko Kiyohara, Tatsuo Kanda and FI analyzed data and wrote the manuscript. Tomoko Kiyohara, KI and TW contributed to experiments using a whole HAV virus. Tomoko Kiyohara, Tatsuo Kanda and VG contributed to the interpretation of the interpretation of the results and took part to the critical revision of the manuscript. All authors read and approved the final manuscript.

Competing interests

The authors declare that they have no competing interests.

Received: 4 June 2010 Accepted: 3 September 2010
Published: 3 September 2010

References

1. FitzSimons D, Hendrickx G, Vorsters A, Damme PV: **Hepatitis A and E: update on prevention and epidemiology.** *Vaccine* 2010, **28**:583-588.
2. Kanda T, Yokosuka O, Imazeki F, Fujiwara K, Nagao K, Saisho H: **Amantadine inhibits hepatitis A virus internal ribosomal entry site-mediated translation in human hepatoma cells.** *Biochem Biophys Res Commun* 2005, **331**:621-629.
3. Widell A, Hansson BG, Oberg B, Nordenfelt E: **Influence of twenty potentially antiviral substances on in vitro multiplication of hepatitis A virus.** *Antiviral Res* 1986, **6**:103-112.
4. Kanda T, Zhang B, Kusov Y, Yokosuka O, Gauss-Müller V: **Suppression of hepatitis A virus genome translation and replication by siRNAs targeting the internal ribosomal entry site.** *Biochem Biophys Res Commun* 2005, **330**:1217-1223.
5. Kanda T, Imazeki F, Nakamoto S, Okitsu K, Yokosuka O: **Internal ribosomal entry-site activities of clinical isolates-derived hepatitis A virus and inhibitory effects of amantadine.** *Hepatol Res* 2010, **40**:415-423.
6. Crance JM, Biziagos E, Passagot J, van Cuyck-Gandre H, Deloince R: **Inhibition of hepatitis A virus replication in vitro by antiviral compounds.** *J Med Virol* 1990, **31**:155-160.
7. Chen Y, Zeng S, Hsu JTA, Horng J, Yang H, Shih S, Chu Y, Wu T: **Amantadine as a regulator of internal ribosome entry site.** *Acta Pharmacol Sin* 2008, **29**:1327-1333.
8. El-Sabbagh OI, Rady HM: **Synthesis of new acridines and hydrazones derived from cyclic b-diketone for cytotoxic and antiviral evaluation.** *Eur J Med Chem* 2009, **44**:3680-3686.
9. Gauss-Müller V, Kusov YY: **Replication of a hepatitis A virus replicon detected by genetic recombination in vivo.** *J Gen Virol* 2002, **83**:2183-2192.
10. Kanda T, Gauss-Müller V, Cordes S, Tamura R, Okitsu K, Wu S, Nakamoto S, Fujiwara K, Imazeki F, Yokosuka O: **Hepatitis A virus (HAV) proteinase 3C inhibits HAV IRES-dependent translation and cleaves the polypyrimidine tract-binding protein.** *J Viral Hepat* 2010, **17**:618-623.
11. Kanda T, Kusov Y, Yokosuka O, Gauss-Müller V: **Interference of hepatitis A virus replication by small interfering RNAs.** *Biochem Biophys Res Commun* 2004, **318**:341-345.
12. Robertson BH, Jansen RW, Khanna B, Totsuka A, Nainan OV, Siegl G, Widell A, Margolis HS, Isomura S, Ito K, Ishizu T, Moritsugu Y, Lemon SM: **Genetic relatedness of hepatitis A strains recovered from different geographical regions.** *J Gen Virol* 1992, **73**:1365-1377.
13. Totsuka A, Moritsugu Y: **Hepatitis A vaccine development in Japan.** In *Viral Hepatitis and Liver Disease.* Edited by: Nishioka K, Suzuki H, Mishiro S. Tokyo: Springer-Verlag; 1994:509-513.
14. Kiyohara T, Totsuka A, Yoneyama T, Ishii K, Ito T, Wakita T: **Characterization of anti-idotypic antibodies mimicking antibody- and receptor-binding sites on hepatitis A virus.** *Arch Virol* 2009, **154**:1263-1269.
15. Kanda T, Steele R, Ray R, Ray RB: **Hepatitis C virus infection induces the beta interferon signaling pathway in immortalized human hepatocytes.** *J Virol* 2007, **81**:12375-12381.
16. Fensterl V, Grotheer D, Berk I, Schlemminger S, Vallbracht A, Dotzauer A: **Hepatitis A virus suppresses RIG-I-mediated IRF-3 activation to block induction of beta interferon.** *J Virol* 2005, **79**:10968-10977.
17. Paulmann D, Magulski T, Schwarz R, Heitmann L, Flehming B, Vallbracht A, Dotzauer A: **Hepatitis A virus protein 2B suppresses beta interferon (IFN) gene transcription by interfering with IFN regulatory factor 3 activation.** *J Gen Virol* 2008, **89**:1593-1604.
18. Yang Y, Liang Y, Qu L, Chen Z, Yi M, Li K, Lemon SM: **Disruption of innate immunity due to mitochondrial targeting of a picornaviral protease precursor.** *Proc Natl Acad Sci USA* 2007, **104**:7253-7258.
19. Cady SD, Schmidt-Rohr K, Wang J, Soto CS, Degrado WF, Hong M: **Structure of the amantadine binding site of influenza M2 proton channels in lipid bilayers.** *Nature* 2010, **463**:689-692.

doi:10.1186/1743-422X-7-212
Cite this article as: Yang *et al.*: Inhibitory effects on HAV IRES-mediated translation and replication by a combination of amantadine and interferon-alpha. *Virology Journal* 2010 **7**:212.

Bmi1 Promotes Hepatic Stem Cell Expansion and Tumorigenicity in Both *Ink4a/Arf*-Dependent and -Independent Manners in Mice

Tetsuhiro Chiba,[1,2,3*] Atsuyoshi Seki,[1,2*] Ryutaro Aoki,[1,2] Hitoshi Ichikawa,[4] Masamitsu Negishi,[1] Satoru Miyagi,[1] Hideyuki Oguro,[1] Atsunori Saraya,[1] Akihide Kamiya,[5] Hiromitsu Nakauchi,[5] Osamu Yokosuka,[2] and Atsushi Iwama[1,3]

We previously reported that forced expression of *Bmi1* (B lymphoma Moloney murine leukemia virus insertion region 1 homolog) in murine hepatic stem/progenitor cells purified from fetal liver enhances their self-renewal and drives cancer initiation. In the present study, we examined the contribution of the *Ink4a/Arf* tumor suppressor gene locus, one of the major targets of *Bmi1*, to stem cell expansion and cancer initiation. *Bmi1*$^{-/-}$ Delta-like protein (Dlk)$^{+}$ hepatic stem/progenitor cells showed de-repression of the *Ink4a/Arf* locus and displayed impaired growth activity. In contrast, *Ink4a/Arf*$^{-/-}$ Dlk^{+} cells gave rise to considerably larger colonies containing a greater number of bipotent cells than wild-type Dlk^{+} cells. Although *Ink4a/Arf*$^{-/-}$ Dlk^{+} cells did not initiate tumors in recipient nonobese diabetic/severe combined immunodeficiency mice, enforced expression of *Bmi1* in *Ink4a/Arf*$^{-/-}$ Dlk^{+} cells further augmented their self-renewal capacity and resulted in tumor formation *in vivo*. Microarray analyses successfully identified five down-regulated genes as candidate downstream targets for Bmi1 in hepatic stem/progenitor cells. Of these genes, enforced expression of *sex determining region Y-box 17* (*Sox17*) in Dlk^{+} cells strongly suppressed colony propagation and tumor growth. *Conclusion:* These results indicate that repression of targets of Bmi1 other than the *Ink4a/Arf* locus plays a crucial role in the oncogenic transformation of hepatic stem/progenitor cells. Functional analyses of Bmi1 target genes would be of importance to elucidate the molecular machinery underlying hepatic stem cell system and explore therapeutic approaches for the eradication of liver cancer stem cells. (HEPATOLOGY 2010;52:1111-1123)

Abbreviations: Alb, albumin; Bmi1, B lymphoma Moloney murine leukemia virus insertion region 1 homolog; CDK, cyclin-dependent kinase; ChIP, chromatin immunoprecipitation; CK7, cytokeratin 7; DDC, 3,5-diethoxycarbonyl-1,4-dihydrocollidine; Dlk, delta-like protein; EGFP, enhanced green fluorescent protein; ESC, embryonic stem cell; GO, Gene Ontology; H2Aub1, monoubiquitinylated histones H2A; HCC, hepatocellular carcinoma; HSC, hematopoietic stem cell; KO, Kusabira-Orange; MACS, magnetic activated cell sorting; NOD/SCID, nonobese diabetic/severe combined immunodeficiency; NSC, neural stem cell; PcG, polycomb group; PRC, polycomb repressive complex; Rb, retinoblastoma protein; RT-PCR, reverse transcription polymerase chain reaction; Sox17, sex determining region Y-box 17.

From the [1]Department of Cellular and Molecular Medicine and [2]Department of Medicine and Clinical Oncology, Graduate School of Medicine, Chiba University, Chiba, Japan; [3]Japan Science and Technology Corporation, Core Research for Evolutional Science and Technology (JST-CREST), Tokyo, Japan; [4]Genetics Division, National Cancer Center Research Institute, Tokyo, Japan; and [5]Division of Stem Cell Therapy, Center for Stem Cell and Regenerative Medicine, Institute of Medical Science, The University of Tokyo, Tokyo, Japan.

Received April 19, 2010; accepted May 31, 2010.

**These authors contributed equally to this work.*

This work was supported in part by grants for Global COE program (Global Center for Education and Research in Immune System Regulation and Treatment) from the Ministry of Education, Culture, Sports, Science and Technology, Japan, and grants from the Chiba Serum Institute Memorial Fund for Health Medical Welfare, Core Research for Evolutional Science and Technology (CREST) of Japan Science and Technology Corporation (JST), the Takeda Science Foundation, and the Uehara Memorial Foundation.

Address reprint requests to: Atsushi Iwama, Department of Cellular and Molecular Medicine, Graduate School of Medicine, Chiba University, 1-8-1 Inohana, Chuo ward, Chiba 260-8670, Japan. E-mail: aiwama@faculty.chiba-u.jp; fax: +81-43-2262191.

Copyright © 2010 by the American Association for the Study of Liver Diseases.

View this article online at wileyonlinelibrary.com.

DOI 10.1002/hep.23793

Potential conflict of interest: Nothing to report.

Additional Supporting Information may be found in the online version of this article.

Polycomb group (PcG) proteins operate as the cellular memory machinery through epigenetic chromatin modifications and are indispensable to the maintenance of cellular identity.[1,2] In particular, Bmi1, a core molecule of polycomb repressive complex 1 (PRC1), plays an important role in the self-renewal of various stem cell systems, including hepatic stem cells.[3]

Recent evidence obtained using stem cell biology–based approaches implies that a rare population of cells in tumors, termed cancer stem cells, possess extreme tumorigenic potential and share several distinctive molecular mechanisms concerning self-renewal, differentiation, and proliferation.[2,4] Of note, it has been demonstrated that Bmi1 is necessary for the maintenance of not only leukemic stem cells but also cancer stem cells in solid tumors.[5,6] Considering that high expression levels of Bmi1 are reported in a wide range of malignancies, Bmi1 could be a general regulator of cancer stem cells as in normal stem cells.

Disruption of the tightly regulated self-renewal process is considered a key early event in carcinogenesis.[7] Enhancement or reacquisition of the self-renewal capability in hematopoietic stem or progenitor cells is essential for leukemogenesis.[8] We also showed that forced expression of *Bmi1* accelerated the self-renewal of hepatic stem/progenitor cells and eventually induced their transformation in an *in vivo* transplant model.[3] However, the molecular machinery underlying the Bmi1-mediated transformation of hepatic stem/progenitor cells remains unclear.

The *Ink4a/Arf* locus, which encodes a cyclin-dependent kinase (CDK) inhibitor, $p16^{Ink4a}$, and a tumor suppressor, $p19^{Arf}$, is a pivotal target of Bmi1.[9] We showed that de-repressed $p16^{Ink4a}$ and $p19^{Arf}$ expression in *Bmi1*-deficient mice was tightly associated with a loss of self-renewing hematopoietic stem cells (HSCs). Deletion of both the *Ink4a* and *Arf* genes substantially restored the self-renewal capacity of *Bmi1*-deficient HSCs. Bmi1 thus regulates HSCs by acting as a critical failsafe against the $p16^{Ink4a}$ and $p19^{Arf}$-dependent senescence pathway.[10,11] Deletion of *Ink4a/Arf* similarly rescues neural stem cell (NSC) self-renewal and frequencies in *Bmi1*-deficient mice, although its effect is reportedly partial.[12] In the oncogenic setting, the Ink4a–retinoblastoma protein (Rb) and Arf-p53 cellular senescence pathways trigger oncogene-induced senescence to eliminate transforming cells that potentially develop into cancer stem cells.[2] Given that enhanced expression of *BMI1* and reduced expression of *INK4A/ARF* are frequently observed in human hepatocellular carcinoma (HCC) samples,[13,14] it would be of importance to understand the contribution of the *Ink4a/Arf* locus to the oncogenic functions of Bmi1 in cancer and search for as-yet-unknown target genes of Bmi1 other than *Ink4a/Arf*.

In the present study, we prepared hepatic stem/progenitor cells from fetal livers of *Bmi1*-deficient and *Ink4a/Arf*-deficient mice and characterized their self-renewal capacity and effects of *Bmi1* overexpression on them. Through these analyses, we found that the *Ink4a/Arf*-independent function of Bmi1 is also essential for its full oncogenic activity in hepatic stem/progenitor cells. Our microarray screening successfully identified candidate downstream targets for Bmi1 in hepatic stem/progenitor cells.

Materials and Methods

Mice. $Bmi1^{+/-}$ mice[15] and $Ink4a\text{-}Arf^{+/-}$ mice (Strain code 01XB1) obtained from Mouse Models of Human Cancers Consortium in the National Cancer Institute (NCI, Frederick, MD) in the C57BL/6 background were used. Nonobese diabetic/severe combined immunodeficient (NOD/SCID) mice were purchased from Sankyo Laboratory (Tsukuba, Japan). All experiments using these mice were performed in accordance with our institutional guidelines for the use of laboratory animals.

Oligonucleotide Array Analysis. Biotin-labeled complementary RNA was prepared with a two-cycle complementary DNA synthesis kit (Affymetrix, Santa Clara, CA) from purified total RNA equivalent to 10,000 cells, and was hybridized to an Affymetrix GeneChip Mouse Genome 430 2.0 array (Affymetrix). The array images were scanned using Affymetrix GeneChip Scanner 3000 7G. The expression value (Signal) for each probe set was calculated using GeneChip Operating Software version 1.4 (Affymetrix). The change value (Signal Log Ratio) and change call (Increase, Marginal Increase, No Change, Marginal Decrease, or Decrease) for each probe set were calculated. Data were obtained for quadrant samples from four independent experiments. To identify differentially expressed genes, we selected probe sets that presented a change call of Increase and a Signal Log Ratio value of ≥ 1 ($\geq$twofold up-regulation) or a change call of Decrease and a Signal Log Ratio value of ≤ -1 ($\geq$twofold down-regulation) in more than three experiments. Moreover, the Welch t test or paired t test was performed to determine significance. Gene Ontology (GO) annotations were performed using the GeneSpring annotation tool (Agilent Technologies, Santa Clara, CA). Microarray data are available at

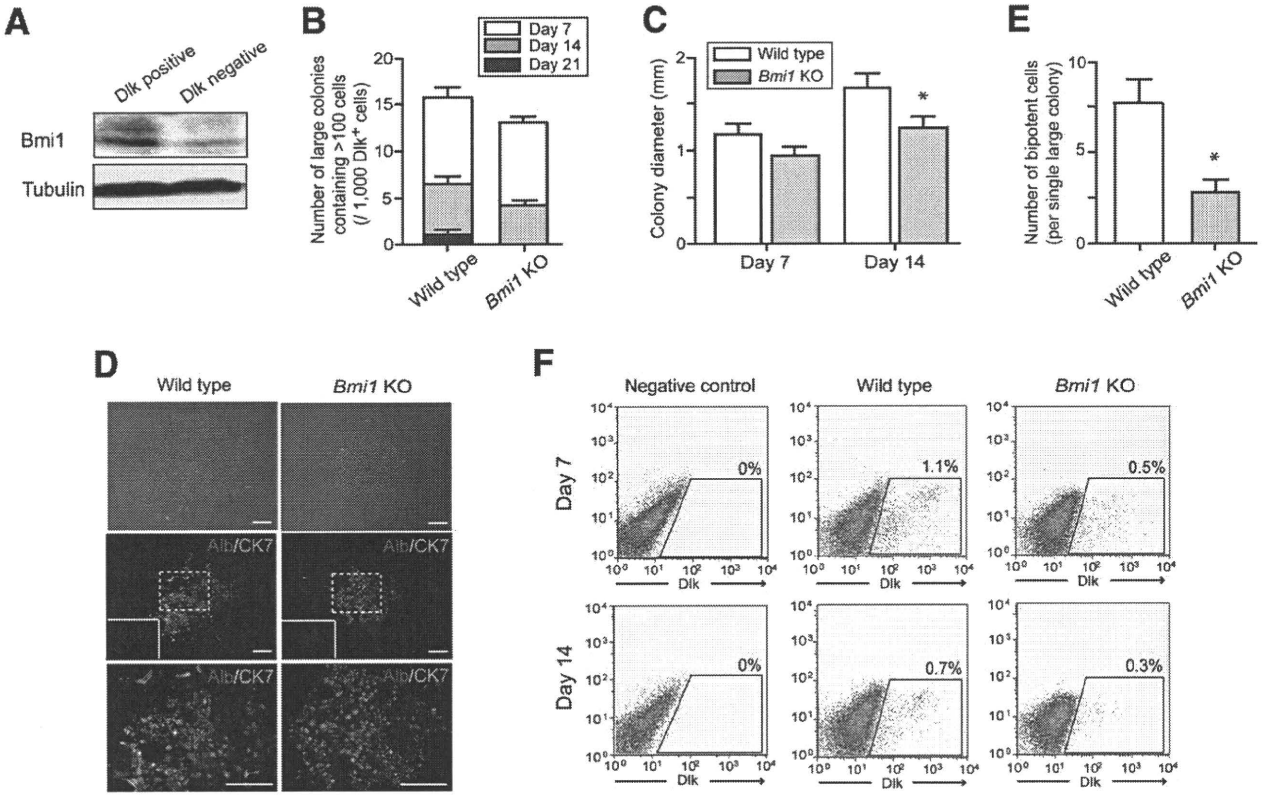

Fig. 1. Colony assays of *Bmi1*$^{-/-}$ hepatic stem cells. (A) Western blot analysis of Bmi1 expression in Dlk^{+} and Dlk^{-} cells purified from wild-type fetal liver. Tubulin was used as a loading control. (B) The number of large colonies containing more than 100 cells at day 7 of culture was traced up to day 21. (C) Colony diameter at days 7 and 14 of culture. *Statistically significant ($P < 0.05$). (D) Bright-field images and immunocytochemical analyses of colonies at day 7 of culture. Alb (red) and CK7 (green) expression was merged. Nuclear DAPI staining (blue) is shown in the insets. (E) The absolute number of Alb^{+}CK7^{+} bipotent cells in large colonies derived from wild-type or *Bmi1*$^{-/-}$ Dlk^{+} cells at day 7 of culture. *Statistically significant ($P < 0.05$). (F) Flow cytometric profiles of colonies derived from wild-type or *Bmi1*$^{-/-}$ Dlk^{+} cells at days 7 and 14 of culture. The percentages of Dlk^{+} cells are shown as mean values for three independent analyses.

http://www.ncbi.nlm.nih.gov/geo/ (accession number: GSE17462).

Other methods are shown in Supporting Materials and Methods.

Results

Impaired Colony Propagation of Bmi1*$^{-/-}$ *Hepatic Stem Cells. Similar to the hematopoietic components, the hepatic components developed normally in *Bmi1*$^{-/-}$ fetal livers and we could recover a comparable number of delta-like protein (Dlk)$^{+}$ hepatic stem/progenitor cells from them. Western blot analysis showed a higher level of Bmi1 expression in wild-type Dlk^{+} cells than Dlk^{-} cells (Fig. 1A). To gain an insight into the role of Bmi1 in hepatic stem cells, we conducted colony assays of wild-type and *Bmi1*$^{-/-}$ Dlk^{+} cells purified by magnetic activated cell sorting (MACS). Flow cytometric analysis revealed that the purity of the sorted Dlk^{+} cells was greater than 90% (Supporting Fig. 1). Approximately 1.5% of wild-type Dlk^{+} cells gave rise to large colonies (consisting of >100 cells) at day 7 of culture. Only a portion of the day 7 colonies kept growing and could be detected as large colonies at days 14 and 21, whereas the majority of colonies stopped expanding and disappeared by days 14 and 21 (Fig. 1B). Although the total number of large colonies did not differ significantly between wild-type and *Bmi1*$^{-/-}$ Dlk^{+} cells at day 7 of culture (Fig. 1B), the diameter of colonies derived from *Bmi1*$^{-/-}$ Dlk^{+} cells was slightly reduced (Fig. 1C). The impeded expansion of *Bmi1*$^{-/-}$ Dlk^{+} cell-derived colonies was obvious at day 14 of culture (Fig. 1B,C). Approximately 10% of large colonies from wild-type Dlk^{+} cells continued to proliferate up to day 21 of culture, whereas no colonies derived from *Bmi1*$^{-/-}$ Dlk^{+} cells expanded beyond day 21 (Fig. 1B).

It has been reported that Dlk^{+} cells are composed of albumin (Alb)$^{+}$ cytokeratin 7 (CK7)$^{+}$ cells and Alb^{+}CK7^{-} cells, and Alb^{+}CK7^{+} cells mainly contribute to the regeneration in retrorsine-treated liver.[16,17] These findings suggest that Alb^{+}CK7^{+} cells, which

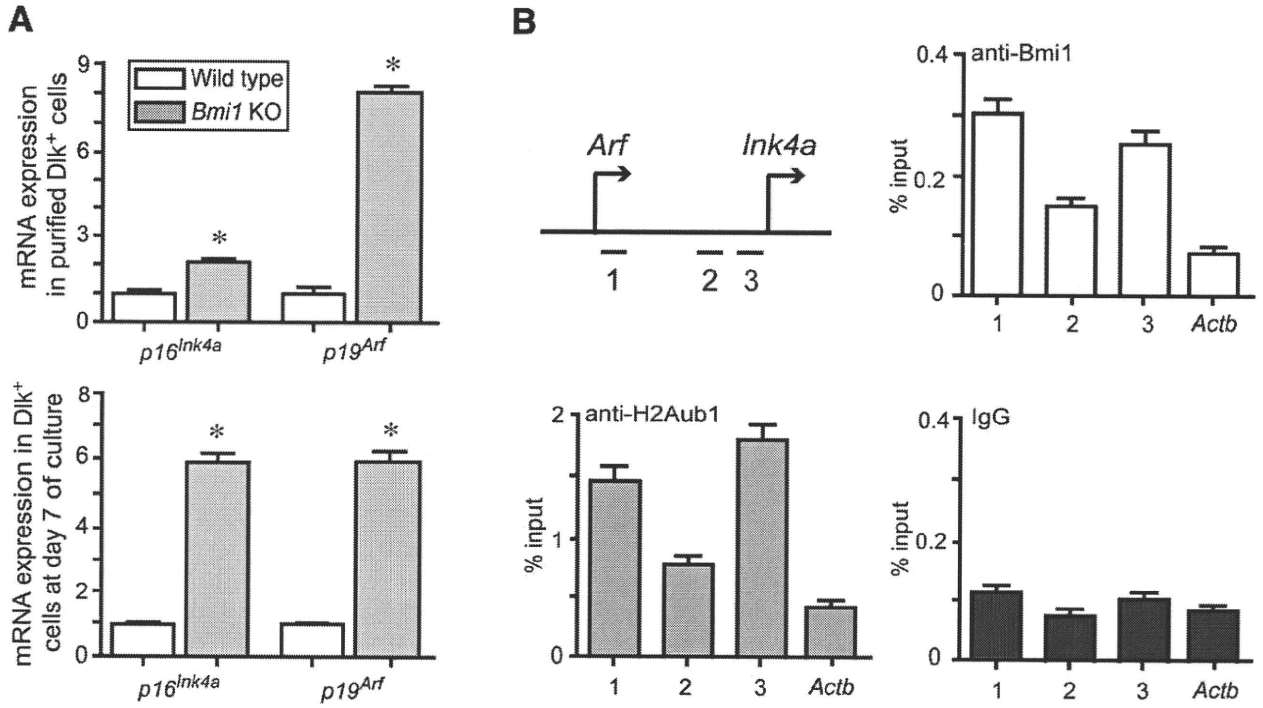

Fig. 2. Regulation of *Ink4a/Arf* expression by *Bmi1*. (A) Real-time RT-PCR analyses of the $p16^{Ink4a}$ and $p19^{Arf}$ genes in freshly purified Dlk^+ cells and Dlk^+ cells cultured for 7 days. *Statistically significant ($P < 0.05$). (B) ChIP analyses of Dlk^+ cells freshly purified from wild-type fetal livers were performed on the *Ink4a/Arf* locus (primer sets 1-3) and the *β-actin* (*Actb*) control promoter region using indicated antibodies. IgG, immunoglobulin G; mRNA, messenger RNA.

have the capacity to give rise to both Alb^+CK7^- and Alb^-Ck7^+ progenies, function as hepatic stem/progenitor cells. Therefore, the quantification of Alb^+CK7^+ impotent cells is one of the approaches to evaluate the content of hepatic stem/progenitor cells, although not all Alb^+CK7^+ cells necessarily have the capacity for bipotential differentiation. Immunocytochemical analyses revealed that the ability of $Bmi1^{-/-}$ Dlk^+ cells to differentiate into Alb^+ hepatocytes and $CK7^+$ cholangiocytes was preserved (Fig. 1D). However, the absolute number of Alb^+CK7^+ bipotent cells were significantly decreased in large colonies derived from $Bmi1^{-/-}$ Dlk^+ cells compared to those in wild-type large colonies (Fig. 1D,E). The absolute number of Alb^+CK7^+ cells per each large colony was 7.6 ± 1.5 and 2.8 ± 0.4, respectively ($P < 0.05$) (Fig. 1E).

Consistent with these findings, flow cytometric analyses demonstrated that the Dlk^+ population in $Bmi1^{-/-}$ colonies decreased rapidly compared to that in wild-type colonies (Fig. 1F). The Dlk^+ fraction in wild-type colonies was 1.1% ± 0.2% at day 7 and 0.7% ± 0.1% at day 14 of culture, whereas that in $Bmi1^{-/-}$ colonies was 0.5% ± 0.1% and 0.3% ± 0.1%, respectively. Conversely, forced expression of *Bmi1* in wild-type Dlk^+ cells significantly promoted colony expansion (Supporting Fig. 2A-C) and increased the Dlk^+ fraction and number of bipotent cells (Supporting Fig. 2D,E).

Oval cells, although their origin is controversial, have been considered stem/progenitor cells in adult liver.[18] Histological analyses demonstrated a drastic decrease in A6-positive oval cell numbers in 3,5-diethoxycarbonyl-1,4-dihydrocollidine (DDC)-treated $Bmi1^{-/-}$ adult liver (Supporting Fig. 3). Together, these findings suggest that Bmi1 plays an important role in the maintenance and expansion of stem/progenitor cells in both fetal and adult livers.

Transcriptional Regulation of the Ink4a/Arf Gene by Bmi1. To examine whether deletion of *Bmi1* causes de-repression of the *Ink4a* and *Arf* genes as observed in HSCs, we conducted real-time reverse transcription polymerase chain reaction (RT-PCR) analyses (Fig. 2A). As expected, messenger RNA levels of *Ink4a* and *Arf* were 2.1-fold and 8.0-fold higher in freshly purified $Bmi1^{-/-}$ Dlk^+ cells than in wild-type Dlk^+ cells, respectively. Colonies derived from $Bmi1^{-/-}$ Dlk^+ cells also showed increased (5.8-fold greater) expression compared to the wild-type colonies. To determine whether Bmi1 is involved in transcriptional regulation of the *Ink4a/Arf* locus, we performed chromatin immunoprecipitation (ChIP) assays using wild-type Dlk^+ cells. ChIP assays demonstrated the binding of

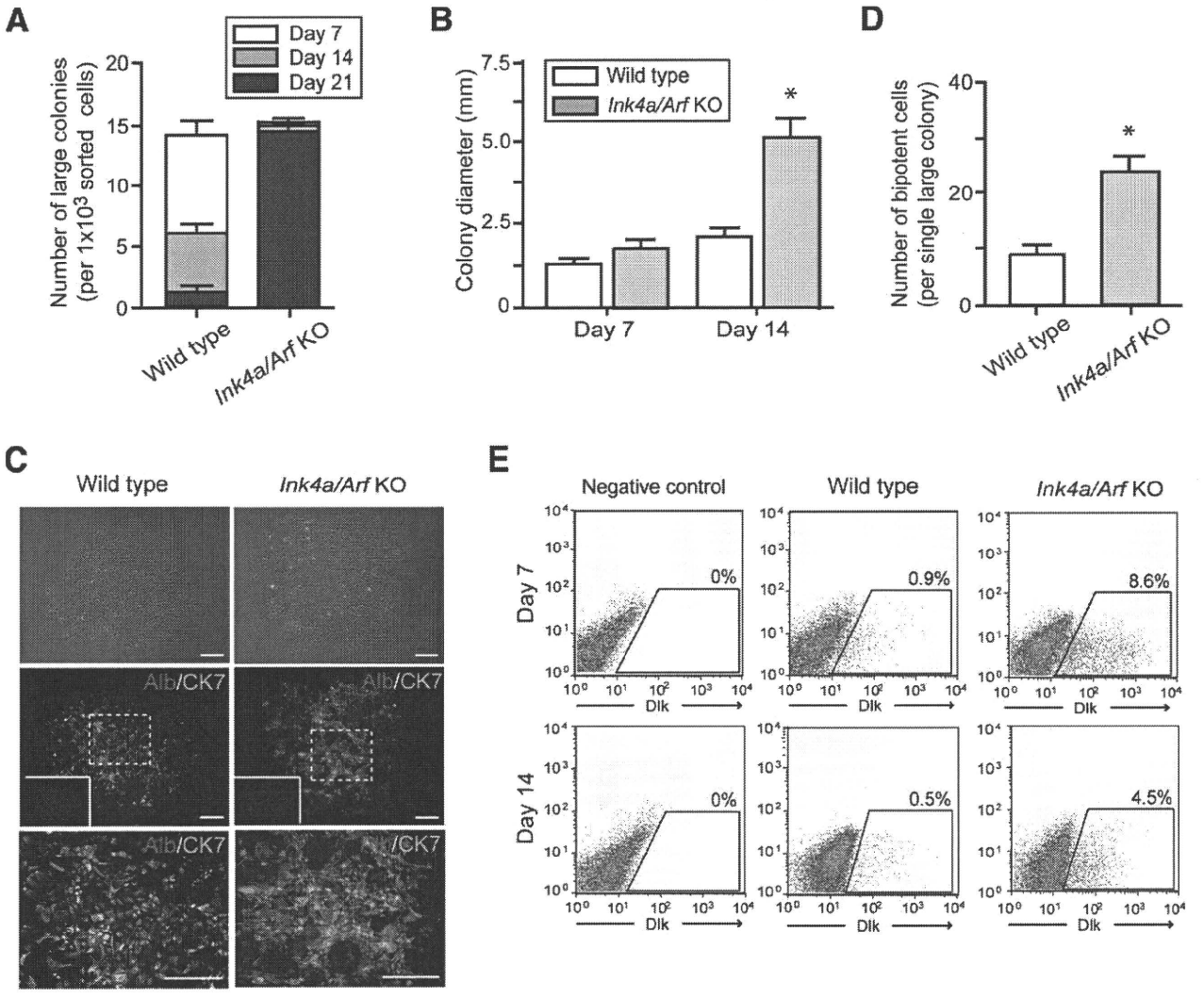

Fig. 3. Colony assays of *Ink4a/Arf*$^{-/-}$ hepatic stem cells. (A) The number of large colonies containing more than 100 cells at day 7 of culture was traced up to day 21. (B) Colony diameter at days 7 and 14 of culture. *Statistically significant ($P < 0.05$). (C) Bright-field images and immunocytochemical analyses of colonies at day 7 of culture. Alb (red) and CK7 (green) expression was merged. Nuclear DAPI staining (blue) is shown in the insets. Scale bar = 200 μm. (D) The absolute number of Alb$^+$CK7$^+$ bipotent cells in large colonies derived from wild-type or *Ink4a/Arf*$^{-/-}$ Dlk$^+$ cells at day 7 of culture. *Statistically significant ($P < 0.05$). (E) Flow cytometric profiles of colonies derived from wild-type or *Ink4a/Arf*$^{-/-}$ Dlk$^+$ cells at days 7 and 14 of culture. The percentages of Dlk$^+$ cells are shown as mean values for three independent analyses.

Bmi1 to the *Ink4a/Arf* locus and increased levels of monoubiquitinylated histone H2A (H2Aub1) (Fig. 2B).

Augmented Colony-Forming Activity of Ink4a/Arf*$^{-/-}$ *Hepatic Stem Cells. To understand the role of the *Ink4a* and *Arf* genes in hepatic stem cells, we next analyzed *Ink4a/Arf*$^{-/-}$ Dlk$^+$ cells in culture. In clear contrast with *Bmi1*$^{-/-}$ Dlk$^+$ cells, *Ink4a/Arf*$^{-/-}$ Dlk$^+$ cells showed pronounced growth activity in culture. The number of large colonies (consisting of more than 100 cells) derived from *Ink4a/Arf*$^{-/-}$ Dlk$^+$ cells was significantly increased compared to that derived from wild-type Dlk$^+$ cells (Fig. 3A,B). By day 14 of culture, *Ink4a/Arf*$^{-/-}$ Dlk$^+$ cells gave rise to distinctly abnormal and large colonies compared to wild-type Dlk$^+$ cells (Fig. 3B,C). More than 95% of large colonies from *Ink4a/Arf*$^{-/-}$ Dlk$^+$ cells further expanded beyond day 21 of culture, although wild-type colonies barely maintained their growth activity (Fig. 3A). Immunocytochemical analyses showed an increase in the proportion and number of Alb$^+$CK7$^+$ bipotent cells in colonies derived from *Ink4a/Arf*$^{-/-}$ Dlk$^+$ cells, particularly in their central area (Fig. 3C). The absolute number of bipotent cells in large colonies derived from wild-type and *Ink4a/Arf*$^{-/-}$ Dlk$^+$ cells at day 7 of culture was 8.2 $\pm$ 2.3 versus 22.7 $\pm$ 4.6 ($P < 0.05$) (Fig.

3D). Flow cytometric analyses revealed that the percentage of Dlk^+ cells in wild-type colonies was 0.9% ± 0.2% at day 7 and 0.5% ± 0.1% at day 14 of culture, although that in *Ink4a/Arf*$^{-/-}$ colonies was 8.6% ± 0.7% and 4.5% ± 0.3%, respectively (Fig. 3E). These findings indicate the enhanced self-renewal capability of hepatic stem cells on the loss of *Ink4a/Arf* expression. Of note, messenger RNA expression of *Bmi1* was comparable between wild-type and *Ink4a/Arf*$^{-/-}$ Dlk^+ cells (data not shown).

As expected, but importantly, the ability of wild-type Dlk^+ cells to propagate colonies was extremely compromised by cotransduction with *Ink4a* and *Arf* retroviruses. Immunocytochemical analyses and flow cytometric analyses showed that the Dlk^+ fraction and bipotent cells were significantly reduced in culture (Supporting Fig. 4).

Enhanced Self-Renewal of Ink4a/Arf*$^{-/-}$ *Hepatic Stem Cells by Bmi1 Overexpression. We previously reported that forced expression of *Bmi1* enhances the self-renewal capacity of hepatic stem/progenitor cells and eventually induces their transformation.[3] To elucidate whether the functional significance of Bmi1 is attributable to the repression of *Ink4a/Arf*, we performed gain-of-function assays of *Bmi1* in *Ink4a/Arf*$^{-/-}$ cells. *Ink4a/Arf*$^{-/-}$ Dlk^+ cells were transduced with either control enhanced green fluorescent protein (*EGFP*) or *Bmi1* 12-18 hours after purification. Enforced expression of Bmi1 was verified by western blot analysis (Fig. 4A). Exogenous Bmi1 in *Ink4a/Arf*$^{-/-}$ Dlk^+ cells did not significantly increase colony number (Fig. 4B). Of note, however, the diameter of *Bmi1*-overexpressing colonies was significantly larger than that of the control colonies (Fig. 4C). Furthermore, flow cytometric analyses showed that the percentage of *Ink4a/Arf*$^{-/-}$ Dlk^+ cells labeled with EGFP was higher in *Bmi1* cultures than in control cultures (22.6% ± 2.3%, 14.0% ± 1.2%, and 8.8% ± 0.7% versus 8.4% ± 1.1%, 3.4% ± 0.5%, and 2.1% ± 0.2% at days 7, 14, and 28 of culture, respectively) (Fig. 4D).

We next carried out single-cell sorting of Dlk^+ cells contained in primary colonies at days 14 and 28 of culture in order to evaluate their self-renewal capacity in terms of replating activity. Dlk^+ cells overexpressing *Bmi1* gave rise to 3.1-fold to 4.0-fold more secondary colonies than the control (Fig. 5A). Secondary colonies were generated in a similar fashion to the original colonies. Immunocytochemical analyses demonstrated that the frequency of Alb^+CK7^+ bipotent cells was significantly higher in secondary colonies derived from Dlk^+ cells collected from the primary *Bmi1*-transduced *Ink4a/Arf*$^{-/-}$ colonies at days 14 and 28 of culture (Fig. 5B,C).

In contrast, *Bmi1*$^{-/-}$*Ink4a/Arf*$^{-/-}$ Dlk^+ cells behaved like *Ink4a/Arf*$^{-/-}$ Dlk^+ cells (Supporting Fig. 5). Although loss of Bmi1 still affected the function of *Ink4a/Arf*$^{-/-}$ hepatic stem/progenitor cells to some extent, these findings indicate that *Ink4a/Arf* is the major target of Bmi1 in hepatic stem cells as in HSCs and NSCs.

Acquisition of Tumorigenic Capacity by Bmi1-Transduced Ink4a/Arf*$^{-/-}$ *Hepatic Stem Cells. We then tested whether the loss of both *Ink4a* and *Arf* is enough for the transformation of hepatic stem cells. Considering that a large number of cells were necessary for transplantations assays, these cells were allowed to form colonies in culture for 28 days. Immunocytochemical analyses showed that more than 90% of cells transduced with *Bmi1* expressed both EGFP, a marker antigen for retrovirus integration, and Flag-tagged Bmi1 (Supporting Fig. 6). Subsequently, a total of 2×10^6 transduced cells were transplanted into the subcutaneous space of NOD/SCID mice (Fig. 5D). Although all the mice transplanted with *Bmi1*-transduced *Ink4a/Arf*$^{-/-}$ Dlk^+ cells developed tumors, none of those transplanted with control *Ink4a/Arf*$^{-/-}$ Dlk^+ cells did. Histological analyses revealed that the subcutaneous tumors consisted of both Alb^+ parenchymal cells and a $CK7^+$ glandular structure (Fig. 5D). The histological finding is consistent with our previous observation in tumors derived from *Bmi1*-transduced wild-type hepatic stem cells.[3] These findings clearly indicate that repression of the *Ink4a* and *Arf* genes is not enough for Bmi1 to achieve its tumorigenic potential in hepatic stem cells.

Gene Expression Analyses of Bmi1-Transduced Ink4a/Arf*$^{-/-}$ *Hepatic Stem Cells. In order to explore novel targets for Bmi1, *Ink4a/Arf*$^{-/-}$ Dlk^+ cells were infected with either the control *EGFP* or *Bmi1*-expressing retrovirus and allowed to form colonies. Dlk^+ cells were purified from colonies at day 28 of culture by cell sorting and subjected to gene expression profiling using oligonucleotide microarrays. We selected genes exhibiting a twofold or greater change with statistical significance in *Bmi1*-transduced *Ink4a/Arf*$^{-/-}$ Dlk^+ cells compared to control *Ink4a/Arf*$^{-/-}$ Dlk^+ cells. As a result, we identified 75 down-regulated genes and 97 up-regulated genes in total (Supporting Table 1). Functional annotation based on GO showed significant enrichment for down-regulated genes which fell into the category "metabolism" and "transport", which included many hepatocyte maturation genes (Fig. 6A). This indicates that Bmi1 strongly suppresses the differentiation and maturation of hepatocytes.

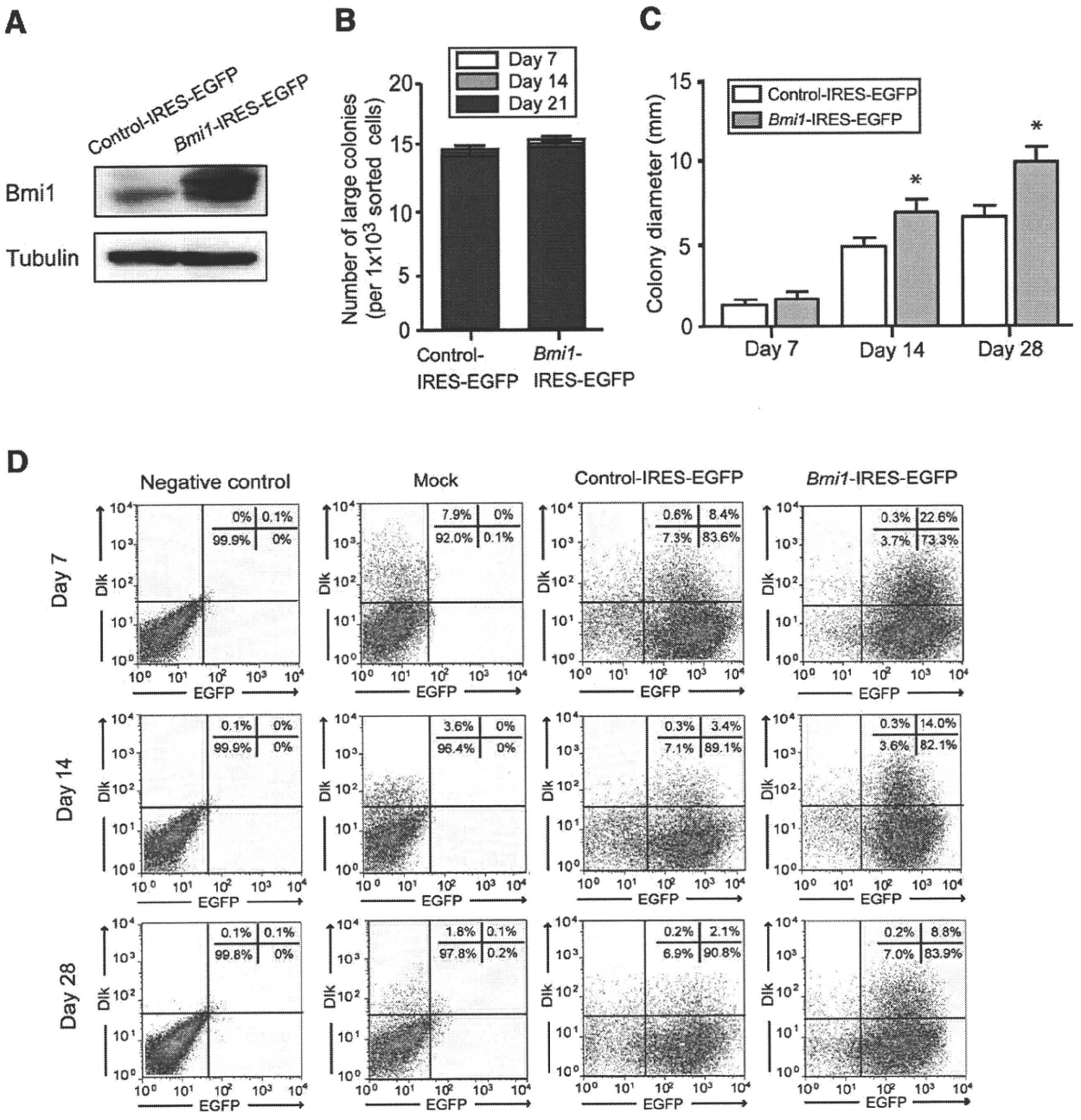

Fig. 4. Gain-of-function assays of *Bmi1* in *Ink4a/Arf*$^{-/-}$ Dlk^{+} cells. (A) Cells transduced with indicated retroviruses were subjected to western blot analysis using anti-Bmi1 and anti-tubulin (loading control) antibodies. (B) The number of large colonies containing more than 100 cells at day 7 of culture was traced up to day 21. (C) The diameter of colonies at days 7, 14, and 28 after transduction of indicated retroviruses. *Statistically significant ($P < 0.05$). (D) Flow cytometric profiles of colonies derived from nontransduced (mock) and *EGFP* or *Bmi1*-transduced *Ink4a/Arf*$^{-/-}$ Dlk^{+} cells at days 7, 14, and 28 in culture. The percentages of each fraction are shown as mean values for three independent analyses.

Recent whole-genome ChIP-on-chip analyses successfully identified genes that are bound by PRC1 and PRC2 complexes in embryonic stem cells (ESCs).[19-21] Boyer et al. reported the genes occupied by PRC1 (Phc1 and Rnf2) and PRC2 (Suz12 and Eed) in murine ESCs.[19] To explore a novel target of Bmi1 in hepatic stem/progenitor cells, we compared the list of down-regulated genes with the ChIP-on-chip data documented by Boyer et al.[19] As a result, five genes namely, *Sox17*, *Irx5*, *Gjb2*, *Shox2*, and *Bhmt2* in the present study appeared to be regulated by both PRC1 and/or PRC2 in ESCs (Fig. 6B). We therefore considered these genes as candidates for direct targets of Bmi1 in hepatic stem cells and performed further analyses on them. In order to confirm the altered expression of these 5 candidate genes, *Ink4a/Arf*$^{-/-}$ Dlk^{+}

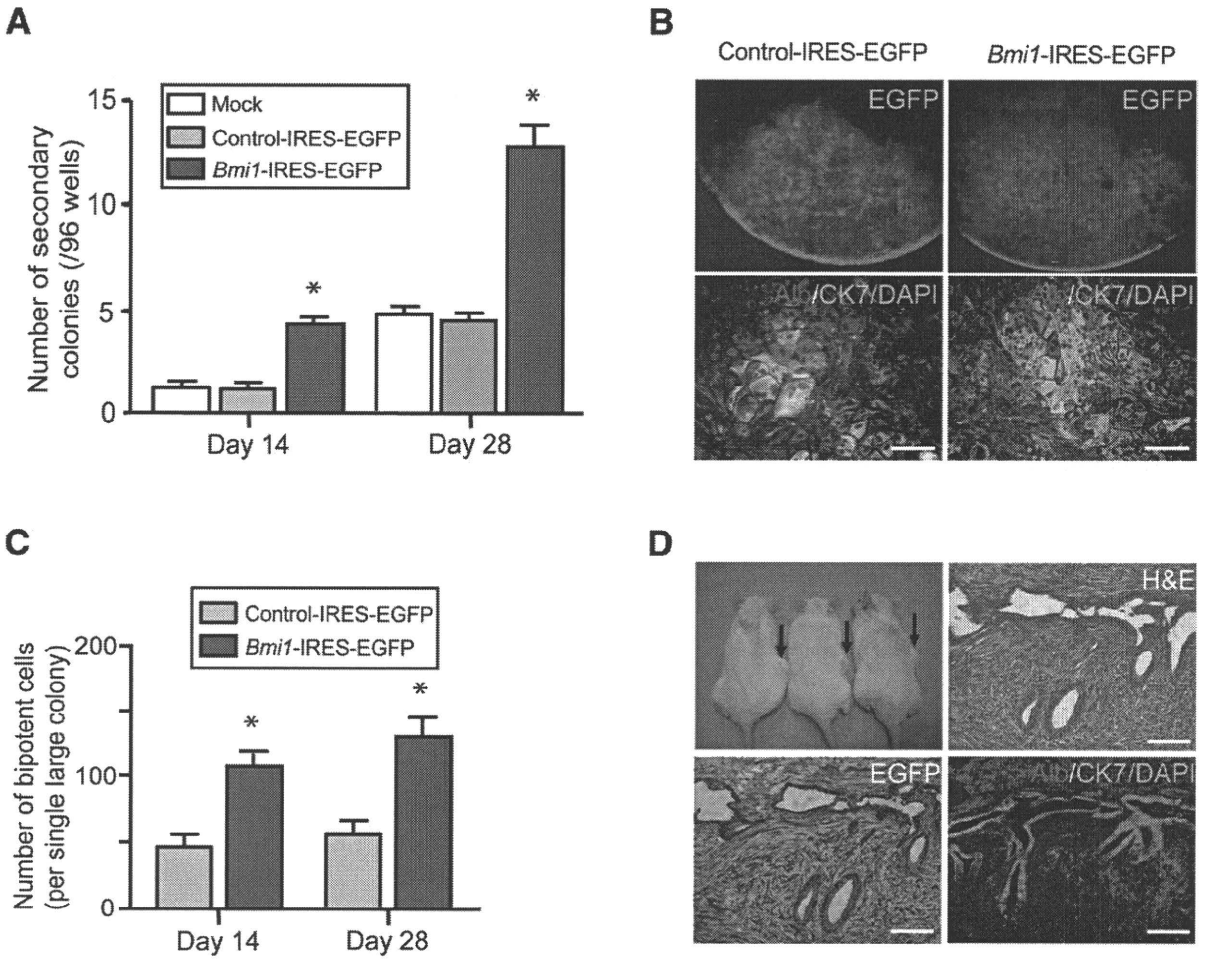

Fig. 5. Replating assays and implantation of *Bmi1*-transduced *Ink4a/Arf*$^{-/-}$ Dlk^{+} cells. (A) Dlk^{+} cells in primary colonies generated from nontransduced (mock) and *EGFP* or *Bmi1*-transduced *Ink4a/Arf*$^{-/-}$ Dlk^{+} cells were clone-sorted at days 14 and 28 of culture and allowed to form colonies. The replating efficiency of Dlk^{+} cells was evaluated by counting the number of secondary colonies containing more than 100 cells 14 days after replating by clone-sorting. *Statistically significant ($P < 0.05$). (B) Fluorescence images (upper panels) and dual immunostaining (lower panels) of secondary clonal colonies derived from *EGFP* or *Bmi1*-transduced *Ink4a/Arf*$^{-/-}$ Dlk^{+} cells at day 28 of culture. Alb (red) and CK7 (green) expression in secondary colonies was merged with nuclear DAPI staining (blue). Scale bar = 100 μm. (C) The absolute number of Alb^{+}CK7^{+} bipotent cells in secondary large colonies at day 14 of subculture. *Statistically significant ($P < 0.05$). (D) *Ink4a/Arf*$^{-/-}$ Dlk^{+} cells were transduced with the control *EGFP* or *Bmi1*-expressing retrovirus and a total of 2×10^{6} transduced cells were transplanted into the subcutaneous space of NOD/SCID mice. *Bmi1*-transduced *Ink4a/Arf*$^{-/-}$ cells formed tumors in the right subcutaneous space of recipient mice (arrows), whereas the same number of control *EGFP*-transduced *Ink4a/Arf*$^{-/-}$ cells did not generate tumors in the left space. Hematoxylin and eosin (H&E) staining of tumors demonstrated histological features compatible with combined hepatocellular and cholangiocellular carcinoma. Immunohistochemical analysis revealed that the tumors were positive for EGFP and consisted of Alb^{+} parenchymal cells (red) and CK7^{+} glandular structures (green). Scale bar = 200 μm.

cells transduced with either control *EGFP* or *Bmi1* were purified from colonies at day 28 of culture and subjected to real-time RT-PCR analyses. The selected five genes exhibited similar expression profiles as in the microarray analysis in *Ink4a/Arf*$^{-/-}$ Dlk^{+} cells (Fig. 6C). Forced expression of *Bmi1* in wild-type Dlk^{+} cells significantly repressed the expression of these genes in a similar fashion to that in *Ink4a/Arf*$^{-/-}$ Dlk^{+} cells (Fig. 6C).

Gain-of-Function Assays of Sox17 in Hepatic Stem Cells. Among candidates for Bmi1 targets, *sex determining region Y-box 17* (*Sox17*) was most severely down-regulated following *Bmi1*-overexpression in hepatic stem cells (Fig. 6C). It has been reported that *Sox17* is highly expressed in the very early definitive endoderm[22] and in hepatocyte-like cells derived from ESCs.[23] These findings prompted us to further examine the role of *Sox17* in hepatic stem cell self-renewal and tumorigenesis. ChIP assays in wild-type Dlk^{+} cells demonstrated specific binding of Bmi1 and an increased level of H2Aub1 at the *Sox17* promoter only in cells transduced with the *Bmi1* retrovirus (Fig. 7A).

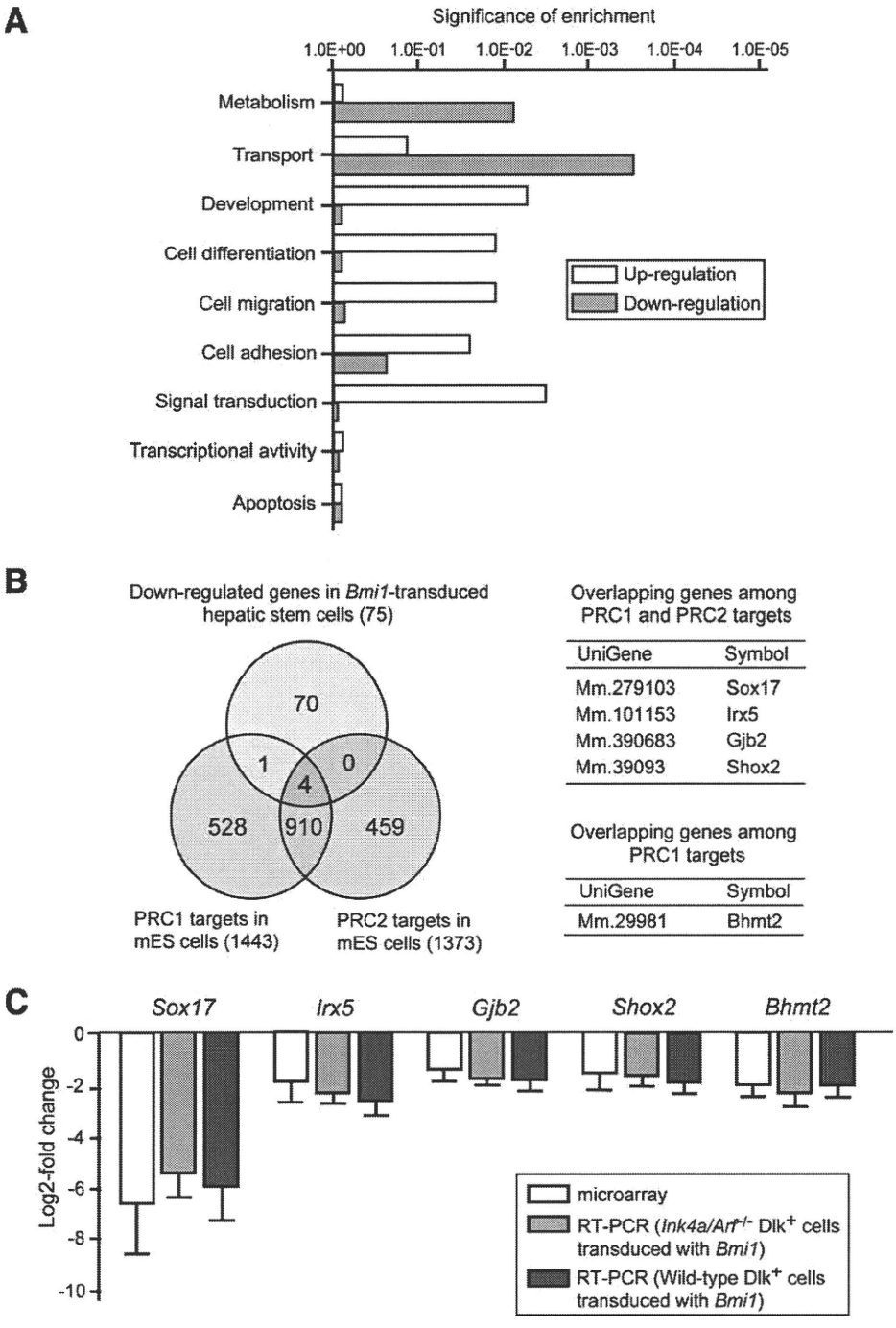

Fig. 6. Gene expression profiles of *Bmi1*-transduced *Ink4a/Arf*$^{-/-}$ Dlk^{+} cells. (A) Gene Ontology (GO) analyses of differentially expressed genes. (B) The overlap of down-regulated genes in the present analysis and PRC targets identified by ChIP-on-chip analyses in mouse ESCs[27] are depicted in a Venn diagram (left panel) and in tables at right. (C) Wild-type and *Ink4a/Arf*$^{-/-}$ Dlk^{+} cells were infected with either the control *EGFP* or *Bmi1*-expressing retrovirus and allowed to form colonies. Dlk^{+} cells were purified from these colonies at day 28 of culture and subjected to real-time RT-PCR analysis. The messenger RNA expression of candidate genes in *Bmi1*-overexpressing cells was compared to that in control cells. The data obtained by microarray analyses are also presented.

All these findings indicate that Bmi1 could directly regulate the expression of *Sox17*.

We next tested the effect of Sox17 in a gain-of-function assay. Overexpression of Sox17 was confirmed by western blotting (Fig. 7B). Enforced expression of *Sox17* in wild-type Dlk^{+} cells severely impaired the formation of colonies and reduced the number as well as size of colonies (Fig. 7C,D). Dlk^{+} cells transduced with *Sox17* did not form any large colonies containing more than 100 cells at day 7 of culture (Fig. 7C) and no colonies expanded beyond day 14 of culture (data not shown). Immunocytochemical analyses showed a decrease in number of Alb^{+}CK7^{+} bipotent cells in colonies derived from Dlk^{+} cells transduced with *Sox17* compared to the control colonies (Fig. 7D,E). Concordant with this, flow cytometric analyses demonstrated that the Dlk^{+} fraction in *Sox17*-transduced colonies was 0.3% $\pm$ 0.1%, much lower that that in wild-type colonies (0.9% $\pm$ 0.2%) (Fig. 7F).

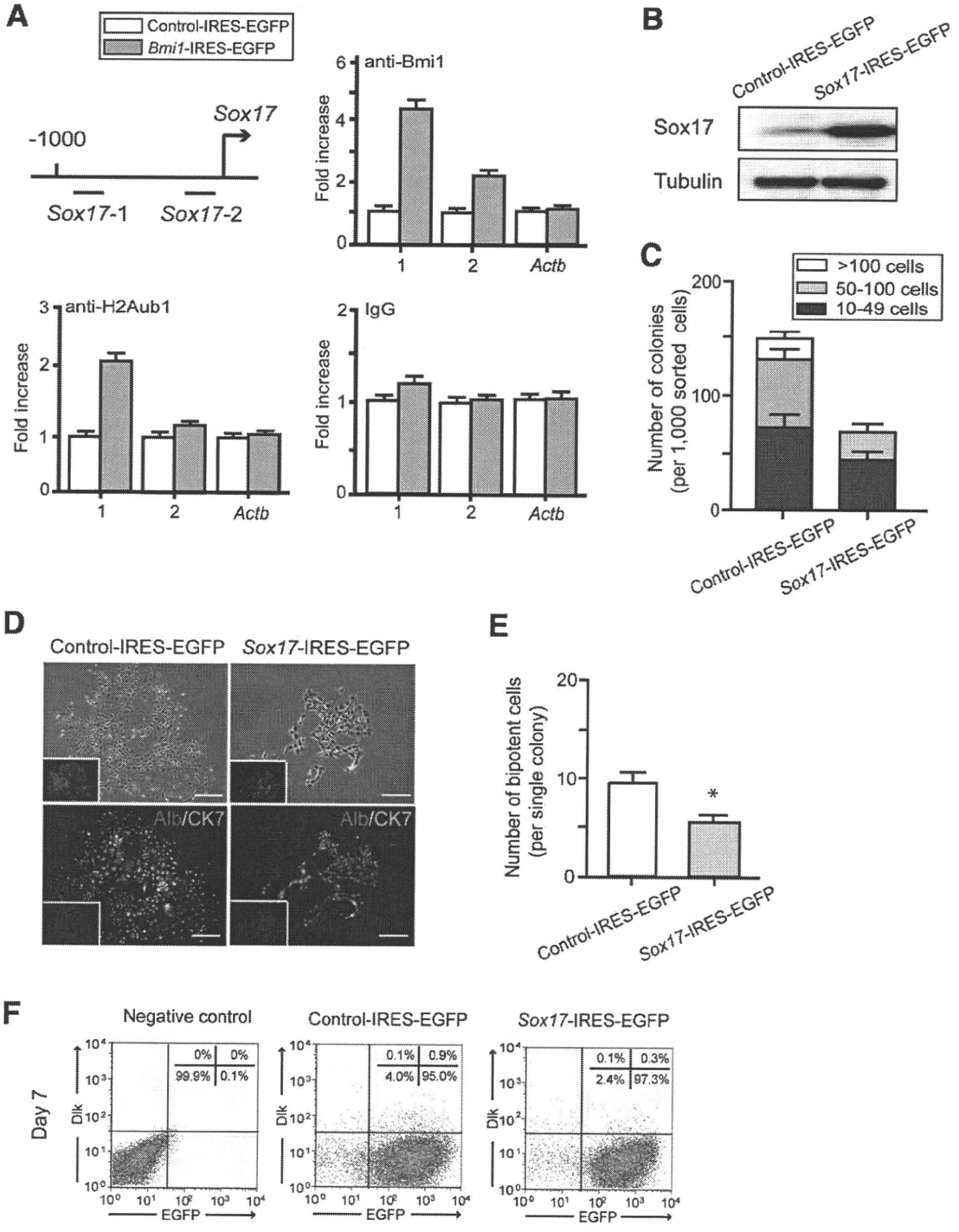

Fig. 7. Gain-of-function assay of *Sox17* in wild-type Dlk$^+$ cells. (A) ChIP analyses of wild-type Dlk$^+$ cells transduced with *EGFP* or *Bmi1* on the *Sox17* locus and *Actb* control promoter region using anti-Bmi1 and anti-H2Aub1 antibodies. *Statistically significant ($P < 0.05$). (B) Western blot analysis in *Sox17*-transduced wild-type Dlk$^+$ cells using anti-Sox17 and anti-tubulin (loading control) antibodies. (C) Enforced expression of *Sox17* in wild-type Dlk$^+$ cells markedly decreased both the total number of colonies and the number of large colonies containing more than 100 cells at day 7 of culture. *Statistically significant ($P < 0.05$). (D) Bright-field images and immunocytochemical analyses of colonies derived from wild-type Dlk$^+$ cells transduced with *Sox17* at day 7 of culture. Alb (red) and CK7 (green) expression was merged. Nuclear DAPI staining (blue) is shown in the insets. Scale bar = 200 μm. (E) The absolute number of Alb$^+$CK7$^+$ bipotent cells in colonies derived from wild-type Dlk$^+$ cells transduced with *Sox17* at day 7 of culture. *Statistically significant ($P < 0.05$). (F) Flow cytometric profiles of colonies derived from *EGFP* or *Sox17*-transduced wild-type Dlk$^+$ cells at day 7 of culture. The percentages of each fraction are shown as mean values for three independent analyses.

To elucidate the impact of *Sox17* on the tumorigenic process driven by *Bmi1*-overexpressing hepatic stem cells, we cotransduced *Ink4a/Arf*$^{-/-}$ Dlk^{+} cells with *Bmi1* and *Sox17*. *Ink4a/Arf*$^{-/-}$ Dlk^{+} cells were simultaneously transduced with *Sox17*-IRES-EGFP and *Bmi1*-IRES-Kusabira-Orange (KO)-expressing retroviral vectors (Supporting Fig. 7A). Flow cytometric profiles demonstrated that more than 90% of cells were successfully cotransduced (Supporting Fig. 7B). A total of 2×10^6 *Ink4a/Arf*$^{-/-}$ cells cotransduced with *Bmi1* and *Sox17* or control *EGFP* were transplanted into the subcutaneous space of NOD/SCID mice. Cotransduction of *Bmi1* and *Sox17* resulted in a significant reduction in tumor volume compared to the cotransduction of *Bmi1* and control *EGFP* (Supporting Fig. 6C). This result indicates that *Sox17* suppresses the tumorigenic activity of *Bmi1*-overexpressing hepatic stem cells.

We then further tested the effect of *Sox17* knockdown in wild-type Dlk^{+} cells (Supporting Fig. 8). *Sox17* knockdown mildly promoted colony expansion and increased the Dlk^{+} fraction and the number of bipotent cells, although its effect was not statistically significant. Transplantation of 2×10^6 *Sox17*-knockdown Dlk^{+} cells did not develop subcutaneous tumors in NOD/SCID mice at all (data not shown).

Discussion

Bmi1, a component of PRC1, regulates the cell cycle, apoptosis and senescence by repressing the *Ink4a/Arf* locus.[5,10] p19^{Arf} suppresses MDM2, which mediates ubiquitin-dependent degradation of p53, and subsequently activates p53 target genes involved in cell cycle arrest and apoptosis, including *p21*.[24] Direct binding of p16^{Ink4a} to CDK4 and CDK6 keeps Rb hypophosphorylated. Hypophosphorylated Rb represses E2F-dependent transcription leading to cell cycle arrest and senescence.[24] Thus, the repression of the *Ink4a/Arf* locus by Bmi1 has a great impact on the maintenance of self-renewing stem cells.

In the present study, *Bmi1*$^{-/-}$ hepatic stem cells showed high levels of *Ink4a* and *Arf* expression and significantly but modestly impaired colony expansion and self-renewal in culture. Although *Bmi1*$^{-/-}$ liver is functionally and histologically normal,[15] oval cell induction following DDC treatment was apparently impaired in *Bmi1*$^{-/-}$ mice (Supporting Fig. 3). Considering the results of gain-of-function (Supporting Fig. 2) and loss-of-function assays of *Bmi1* (Fig. 1), the possibility exists that redundancy among other PcG molecules such as Mel18 weakens the phenotype of *Bmi1*$^{-/-}$ hepatic stem cells in developing and adult liver.[25] In clear contrast, *Ink4a/Arf*$^{-/-}$ hepatic stem cells exhibited enhanced colony formation and retained a large Dlk^{+} population in culture compared to the wild type. Furthermore, deletion of both *Ink4a* and *Arf* largely restored the impaired self-renewal capacity of *Bmi1*$^{-/-}$ hepatic stem cells (Supporting Fig. 5). These findings indicate that *Ink4a/Arf* is the major target of Bmi1 in hepatic stem cells as in HSCs and NSCs.[11,12]

Bmi1 is also essential for cancer stem cells as demonstrated in a mouse leukemia model as well as in a mouse lung tumor model generated by the expression of a mutant K-ras gene in bronchioalveolar stem cells.[5,26] In addition, we previously demonstrated that forced expression of *Bmi1* promotes the self-renewal of hepatic stem/progenitor cells and contributes to malignant transformation.[3] All these findings highlight the important role of Bmi1 in both the development and maintenance of cancer stem cell systems. Of interest, an *Ink4a/Arf*-independent contribution of Bmi1 to not only self-renewal in neural stem cells but also tumorigenesis in a mouse model for glioma has been reported.[27,28] The current *in vivo* transplant assays ascertained that *Bmi1*-transduced *Ink4a/Arf*$^{-/-}$ Dlk^{+} cells but not control *Ink4a/Arf*$^{-/-}$ Dlk^{+} cells acquire tumorigenic potential. *Bmi1*-transduced *Ink4a/Arf*$^{-/-}$ Dlk^{+} cells showed an augmented self-renewal capability as evident from the higher replating efficiency in the single cell-sorting analysis compared to *Ink4a/Arf*$^{-/-}$ Dlk^{+} cells. These results clearly demonstrated that repression of the *Ink4a/Arf* locus only does not directly drive tumor initiation in hepatic stem cells. Considering that *Ink4a/Arf*$^{-/-}$ mice barely developed primary liver tumors in their lifetime,[29] repression of additional targets of *Bmi1* may be needed in cancer initiation.

To evaluate the impact of Bmi1 on gene expression in hepatic stem cells and to explore the additional targets of Bmi1 related to tumorigenesis, we conducted an oligonucleotide array analysis using *Bmi1*-transduced *Ink4a/Arf*$^{-/-}$ Dlk^{+} cells and the control *Ink4a/Arf*$^{-/-}$ Dlk^{+} cells. The screening of more than 39,000 transcripts successfully identified 75 down-regulated and 97 up-regulated genes (Supporting Table 1). As expected, enforced expression of *Bmi1* contributed to the maintenance of stemness features and suppression of differentiation-related genes. The present analysis revealed gene expression to be up-regulated for the hepatic stem cell markers *Prom1* (*CD133*) ($P = 0.041$) and *EpCAM* ($P = 0.017$) and down-regulated for the hepatocyte differentiation markers *Cps1* ($P = 0.010$), Mat1a ($P = 0.011$), and *Gjb2* (*Cx26*) ($P = 0.010$).